

WIND STUDIES OF BANK OF AMERICA WORLD
HEADQUARTERS BUILDING

PART II

WIND TUNNEL STUDY

by

R. D. Marshall, Department of Civil Engineering

J. E. Cermak, Professor-in-Charge, Fluid Mechanics Program

under contract with

Metronics Associates, Inc.
3201 Porter Drive
Stanford Industrial Park
Palo Alto, California
94304

for

Architects for Bank of America World Headquarters Building
1620 Montgomery Street
San Francisco, California
94111

Fluid Dynamics Program
Fluid Dynamics and Diffusion Laboratory
College of Engineering
Colorado State University
Fort Collins, Colorado
80521

October, 1966

CER66-67RDM-JEC 19

ABSTRACT

Mean pressure distributions were obtained for three wind directions (S, SW and W) using a 1:200 scale model of the proposed structure submerged in a uniform air stream and for two wind directions (S and W) using a 1:600 scale model submerged in a turbulent boundary layer. Surface pressure-difference fluctuations were investigated at selected points on the model having a separation of three-quarters of the glass-panel span for both uniform and boundary-layer flows.

The observed base pressures for this structure were appreciably smaller in magnitude than would be expected for a similar structure having smooth walls. Surface pressure-difference fluctuations on the order of one dynamic pressure were observed for certain critical wind directions and these fluctuations exhibited a marked increase in intensity when the flow was made turbulent.

Characteristic eddy-shedding frequencies for the gross structure and general flow patterns at street level were obtained for a range of velocities and turbulence intensities. Strouhal numbers for both uniform and boundary-layer flows compared favorably with published values for structures of similar shape. An intense downflow on the windward face of the model was observed for boundary-layer flows.

ACKNOWLEDGEMENTS

The authors wish to acknowledge the many helpful suggestions and criticisms of Dr. J. S. Ostrowski during the wind tunnel study and in the interpretation of the results.

To Dr. W. A. Perkins, the authors also express their sincere thanks for his many contributions.

TABLE OF CONTENTS

	<u>Page</u>
ABSTRACT.	ii
ACKNOWLEDGEMENTS	iii
LIST OF TABLES	v
LIST OF FIGURES.	vi
LIST OF SYMBOLS	viii
I. INTRODUCTION	1
II. DESCRIPTION OF WIND TUNNEL STUDY	1
A. Models	2
B. Wind Tunnel - Model Arrangement	2
C. Equipment	3
III. DISTRIBUTION OF MEAN PRESSURE	4
IV. SURFACE PRESSURE-DIFFERENCE FLUCTUATIONS	18
V. CHARACTERISTIC EDDY-SHEDDING FREQUENCIES .	26
VI. GENERAL FLOW PATTERNS AROUND BUILDING . . .	29
VII. SUMMARY OF FINDINGS AND RECOMMENDATIONS .	32
REFERENCES	34
<u>APPENDIX A</u>	
Equipment List	35

LIST OF TABLES

<u>Table</u>		<u>Page</u>
1	Pressure Coefficients - Uniform Flow (1:200 Scale Model)	7
2	Pressure Coefficients - Uniform Flow (1:600 Scale Model)	15
3	Pressure Coefficients - Turbulent Boundary- Layer Flow (1:600 Scale Model).	16
4	Surface Pressure-Difference Fluctuations- Uniform Flow	20
5	Surface Pressure-Difference Fluctuations- Turbulent Boundary-Layer Flow.	22
6	Turbulence Intensities (1:200 Scale Model)	24
7	Strouhal Numbers.	28
8	Turbulence Intensities (1:600 Scale Model)	31

LIST OF FIGURES

<u>Figure</u>		<u>Page</u>
1	1:200 Scale Model	38
2	1:600 Scale Model	39
3	Rotary Table	39
4	San Francisco - Southwest	40
5	San Francisco - West	40
6	San Francisco - West (Looking upstream)	41
7	Low-Speed Wind Tunnel	42
8	Pressure Tap Arrangement (1:200 scale model) .	43
9	Pressure Tap Arrangement - Levels A, B, C, D, E, F & R	44
10	Pressure Tap Arrangement - Level G	45
11	Pressure Tap Arrangement - Level H	46
12	Pressure Tap Arrangement - Levels J, K & L .	47
13	Pressure Tap Arrangement (1:600 scale model) .	48
14	Roof Plan (1:600 scale model)	49
15	Pressure Coefficient Distribution - South Side . .	50
16	Pressure Coefficient Distribution - South Side . .	51
17	Pressure Coefficient Distribution - North Side . .	52
18	Pressure Coefficient Distribution - West Side . .	53
19	Pressure Coefficient Distribution - East Side. . .	54
20	Oscillogram - Surface Pressure-Difference Fluctuation	55

LIST OF FIGURES - Continued

<u>Figure</u>		<u>Page</u>
21a	Flow Pattern - Azimuth = 180° - $U_o = 30$ ft/sec . .	56
21b	Flow Pattern - Azimuth = 180° - $U_o = 60$ ft/sec . .	56
22a	Flow Pattern - Azimuth = 270° - $U_o = 30$ ft/sec . .	57
22b	Flow Pattern - Azimuth = 270° - $U_o = 60$ ft/sec . .	57
23a	Mean Velocity Profile - S. F. South - Sutter St. . .	58
23b	Mean Velocity Profile - S. F. South - Sutter St. . .	59
24a	Mean Velocity Profile - S. F. South - Sutter St. . .	60
24b	Mean Velocity Profile - S. F. South - Sutter St. . .	61
25	Mean Velocity Profile - S. F. West - Taylor St. . .	62
26a	Mean Velocity Profile - S. F. West - Grant St. . .	63
26b	Mean Velocity Profile - S. F. West - Grant St. . .	64
27a	Mean Velocity Profile - S. F. West - Grant St. . .	65
27b	Mean Velocity Profile - S. F. West - Grant St. . . .	66

SYMBOLS

Symbol

C_p	Pressure coefficient $\left(\frac{p - p_{\text{ref}}}{\rho U_o^2 / 2} \right)$
D	Characteristic length
Δh	Local dynamic pressure head, mm Hg.
Δh_o	Free-stream dynamic pressure head, mm Hg.
n	Frequency, cycles/sec
p'	Pressure difference, lbs/ft ²
S	Strouhal number $\left(\frac{nD}{U} \right)$
U	Local mean velocity, ft/sec
U_o	Free-stream velocity, ft/sec
u	Fluctuating component of velocity, ft/sec
y	Distance perpendicular to boundary
δ	Boundary-layer thickness
ρ	Mass density of air, slugs/ft ³
σ	Standard deviation

I. INTRODUCTION

The investigation described in this report constitutes Phase II of the program of wind studies of the Bank of America World Headquarters Building (BAWHB). Phase I of the program is a meteorological study of the proposed site which was undertaken by Metronics Associates, Inc. of Palo Alto, California.

Since model studies generally can only be carried out at smaller Reynolds numbers than those for the full-scale structure, the absence of aerodynamic scale effect is essential for dynamic similarity. Fortunately this effect is not very large except for structures of rounded cross-section. Gustiness of the wind and variation of velocity with height must also be considered if the full-scale flow is to be modeled in a wind tunnel. This is accomplished by generating a turbulent boundary layer of proper thickness over a suitable roughness placed on the tunnel floor upstream of the building model.

This wind tunnel model study of the proposed structure was made to determine the wind induced pressure distributions over the building surface for the purpose of computing forces and moments. Because of the unique form of the exterior walls and the unusually large window panels to be employed, an exploratory study of the surface pressure-difference fluctuations was conducted for various combinations of wind speed, direction and intensity of turbulence. Characteristic eddy-shedding frequencies of the gross structure as well as general flow patterns around the base of the structure are also presented herein.

II. DESCRIPTION OF WIND TUNNEL STUDY

In this section a brief description is given of the models, the wind tunnel - model arrangement and the equipment used to carry out this study.

A. Models

Two models were used in this study, a 1:200 scale model supplied jointly by the architect and Colorado State University and a 1:600 scale model supplied by the architect.

The 1:200 scale model of the BAWHB was constructed of "Lucite" with two removable sides and top to facilitate installation of pressure taps and transducers. Since the main purpose of this model was to investigate local flow instabilities produced by the building geometry, it was highly detailed. Surrounding buildings in an area bounded by Sacramento, Sansome, Post and Stockton Streets were constructed of styrafoam and were mounted on plywood sheets. This portion of the model was supplied by Colorado State University. By dividing the overall model into sections of proper shape, it was possible to install strips of the model corresponding to the three wind directions investigated.

The 1:600 scale model was also constructed of "Lucite" but with much less detail. This model was equipped with pressure taps and had a removable top to allow installation of pressure transducers. The surrounding buildings and topography were modeled in detail over an area bounded by Washington, Battery, Sutter and Taylor Streets. Photographs of these models are reproduced in Figs. 1 and 2.

B. Wind Tunnel - Model Arrangement

The 1:200 scale model of the BAWHB was mounted on an 18 in. diameter steel plate which in turn was mounted on a rotary table located beneath the tunnel floor. The rotary table was equipped with an electric drive motor which allowed the model to be rotated at a constant rate while the pressure-difference fluctuations were monitored. This entire system was mounted in a massive concrete base isolated from building vibrations by rubber pads. This was particularly important

for those portions of the study which required the mounting of pressure transducers inside the model. A photograph of the rotary table and pressure tubing used to measure mean pressures is reproduced in Fig. 3.

For those portions of the study which required a turbulent boundary-layer flow approaching the 1:200 scale model, the upstream portion of the tunnel floor (about 28 ft) was covered with modular brick. (2-1/4 x 3-5/8 x 7-5/8 in.) An attempt was made to duplicate building height and density including the topography of Nob Hill for each direction studied. The completed model extended to China Basin for the south wind, to Civic Center for the southwest wind, and to Lafayette Square for the west wind. Although the site investigation of meteorological conditions had not been completed at the time the wind tunnel study was in progress, it was determined that these three wind directions were of major interest. Wind directions were referenced to the San Francisco Street system in the vicinity of the building site rather than to true north. A porous barrier was placed at the tunnel entrance to augment the boundary-layer thickness. Typical views of the model and upstream roughness are shown in Figs. 4-6.

A similar procedure was followed for the 1:600 scale model but in this case the upstream barrier was not required since the boundary-layer thickness corresponded to a prototype boundary-layer thickness of 1600 ft.

Since the wind tunnel ceiling is not adjustable, it was necessary to carry out this study in flows having non-zero pressure gradients. To correct the data for this effect, a series of pressure taps was installed along the tunnel ceiling. The location of these taps and the location of the model are shown in Fig. 7.

C. Equipment

The low-speed wind tunnel of the Fluid Dynamics and Diffusion

Laboratory is equipped with an instrument carriage which allows continuous traverses to be made in the lateral and vertical directions. A Prandtl tube mounted on this carriage and connected to a "Trans-Sonics" electronic manometer was used to obtain continuous vertical profiles of wind speed. The electrical outputs of the manometer and the instrument carriage position potentiometers were fed into an 8-1/2 x 11 in. X-Y plotter.

The 1:200 scale model was fitted with 161 pressure taps having an inside diameter of 0.035 in. and connected to the electronic manometer with 10 ft lengths of 1/8 in. I.D. vinyl tubing. Some of these taps were arranged in pairs so that pressure-difference fluctuations could be measured. In this case "Statham" pressure transducers were mounted inside the model and closely connected to the pressure taps using the same 1/8 in. I.D. tubing. The transducers with associated pressure tubing had a flat frequency response to about 100 cycles/sec.

A similar procedure was followed with the 1:600 scale model, but in this case the tubing had an inside diameter of 1/16 in. and the tube length was 4 ft. The pressure taps had an inside diameter of 0.063 in.

Turbulence data were obtained with a hot-wire anemometer developed at the Fluid Dynamics and Diffusion Laboratory. The sensing element was a silver plated, 0.0002 in. diameter tungsten wire having a cold resistance of 5 ohms. A list of equipment used in this study along with the pertinent operating characteristics is given in Appendix A.

III. DISTRIBUTION OF MEAN PRESSURE

Mean pressure distributions over the building surface for the purpose of computing forces and moments produced by wind loading were obtained with the 1:200 scale model. These mean pressures

were measured in a uniform air stream having a mean flow speed of 30 ft/sec and are presented in Table 1 and Figs. 15-19 as a dimension-

less ratio $C_p = \frac{p-p_{ref}}{\rho U_o^2/2}$

where

p = surface pressure

p_{ref} = ambient static pressure

ρ = mass density of air

U_o = ambient wind speed

The pressure tap locations are given in Figs. 8-12.

Since the prototype Reynolds number will be about 800 times that of the model under high wind conditions, invariance of flow pattern with Reynolds number is necessary if the model pressure coefficients are to be applicable to the prototype. This is generally the case for flow over a cross-section with sharp edges such as the BAWHB. To confirm this, the pressure coefficients for one wind direction (south) were obtained for speeds of 30 and 50 ft/sec. These coefficients are also presented in Table 1 for comparison. No significant difference in the two sets of coefficients is observable.

Since the cross-section of the wind tunnel is 6 ft x 6 ft, introduction of the 1:200 scale model into the air stream produced a substantial tunnel blockage. This caused the observed base pressures to be much lower than they would have been had the effects of the restraining tunnel walls been absent. The pressure coefficients presented in Table 1 have been adjusted for this blockage effect.

To obtain a check on the 1:200 scale model data and to determine the effect of a velocity gradient on the mean surface pressures, a 1:600 scale model was placed in a uniform air stream and in a turbulent boundary-layer flow. The resulting pressure coefficients are

presented in Tables 2 and 3 and the pressure tap arrangement for the 1:600 scale model is shown in Figs. 13 and 14. The boundary-layer thickness over the model was 32 in. which corresponds to a prototype thickness of 1600 ft. Tunnel blockage in this case was negligible.

Architectural revisions which tended to make the building more symmetrical about a N-S axis were made after this phase of the study had been completed. Just what effect these revisions might have on the surface pressure distributions is not known. It was also discovered that the east and west faces had been interchanged when the 1:200 scale model was constructed. However, since the two sides are identical except for the elevations of the set-backs, it is doubtful that this will require any change in the observed distributions.

In order to determine the effect of the unusual surface features of the structure on the base pressures, the 1:600 model was covered with cardboard sheets to simulate a structure having smooth walls. On the basis of several pressure measurements it was found that the rough walls reduce the base pressures by as much as 20%.

TABLE 1
Pressure Coefficients - Uniform Flow
(1:200 scale model)

$$C_p = \frac{p - p_{ref}}{\rho U_o^2 / 2}$$

Tap No.	Azimuth Angle U_o - ft/sec	180 30	0 30	180 50	0 50	45 30	135 30	225 30	315 30	270 30	90 30
A	1	-0.85	-0.91	-0.88	-0.89			-0.83	-0.77	-0.58	0.70
	2	-0.85	-0.83	-0.86	-0.81			-0.74	-0.85	-0.84	-1.14
	3	0.02	-0.85	-0.04	-0.87			-0.27	-0.74	-0.33	-1.17
	4	-0.01	-0.83	-0.06	-0.89			-0.14	-0.74	-0.44	-1.16
	5	-0.91	-0.96	-0.87	-0.99			0.12	-0.47	0.83	-0.55
	6	-0.91	-0.85	-0.86	-0.85			-0.79	0.68	-0.03	-0.63
	7	-0.85	0.67	-0.82	0.67			-0.97	0.25	-1.17	-0.61
	8	-0.85	0.41	-0.85	0.47			-0.65	0.44	-1.13	-0.93
	9	-0.85	0.18	-0.84	0.15			-0.86	-0.48	-1.00	-1.11
B	1	-0.86	-0.85	-0.86	-0.89			-0.85	-0.80	-0.60	-0.35
	2	-0.89	-0.85	-0.86	-0.87			-0.85	-0.85	-0.83	-1.23
	3	-0.70	-0.86	-0.76	-0.90			-0.89	-0.71	-0.39	-1.16
	4	-0.71	-0.88	-0.73	-0.89			-0.83	-0.67	-0.53	-1.17
	5	-0.89	-1.00	-0.85	-0.98			-0.26	-0.07	-0.63	-0.56
	6	-0.91	-0.97	-0.84	-0.95			-0.71	0.42	-0.48	-0.60
	7	-0.85	-0.61	-0.85	-0.66			-0.83	0.32	-1.16	-0.54
	8	-0.88	-1.00	-0.85	-1.02			-0.68	-0.44	-1.13	-0.86
	9	-0.86	-0.82	-0.85	-0.87			-0.77	-0.80	-0.97	-1.11

TABLE 1 - Continued

Tap	Azimuth Angle	180	0	180	0	45	135	225	315	270	90
No.	U_o - ft/sec	30	30	50	50	30	30	30	30	30	30
C	1	-0.88	-0.86	-0.89	-0.88			-0.88	-0.76	-0.59	-1.30
	2	-0.85	-0.92	-0.90	-0.86			-0.86	-0.80	-0.73	-1.17
	3	-0.91	-0.89	-0.91	-0.87			-1.17	-0.73	-0.46	-1.14
	4	-0.91	-0.89	-0.92	-0.89			-1.15	-0.70	-0.61	-1.16
D	1	-0.82	-0.82	-0.86	-0.85			-0.83	-0.76	-0.64	0.66
	2	-0.82	-0.86	-0.85	-0.87			-0.85	-0.77	-0.66	0.67
	3	-0.79	-0.86	-0.85	-0.89			-0.82	-0.77	-0.69	0.73
	4	0.49	-0.83	0.51	-0.87			0.14	-0.73	-0.22	-1.16
	5	0.50	-0.86	0.53	-0.86			0.41	-0.68	-0.36	-1.17
	6	0.46	-0.86	0.50	-0.88			0.18	-0.67	-0.67	-1.17
	7	0.46	-0.86	0.48	-0.87			0.33	-0.65	-1.02	-1.03
	8	0.46	-0.83	0.48	-0.90			0.36	-0.65	-1.09	-0.87
	9	0.46	-0.85	0.48	-0.86			0.56	-0.64	-1.16	-0.67
	10	0.39	-0.89	0.41	-0.89			0.76	-0.65	-1.20	-0.66
	11	-0.76	-0.86	-0.80	-0.91			0.93	-1.02	-1.27	-0.79
	12	-1.18	-0.94	-1.17	-0.90			-0.07	-0.46	0.74	-0.61
	13	-1.15	-1.11	-1.17	-0.98			0.04	0.09	0.72	-0.57
E	1	-0.82	-0.85	-0.84	-0.84			-0.79	-0.78	-0.66	0.79
	2	-0.82	-0.85	-0.84	-0.84			-0.79	-0.78	-0.67	0.82
	3	-0.69	-0.86	-0.69	-0.86			-0.89	-0.78	-0.74	-0.31
	4	-0.67	-0.85	-0.70	-0.86			-0.85	-0.78	-0.80	-0.82
	5	0.73	-0.85	0.72	-0.86			0.65	-0.71	-0.28	-1.17

TABLE 1 - Continued

Tap No.	Azimuth Angle U_o - ft/sec	180 30	0 30	180 50	0 50	45 30	135 30	225 30	315 30	270 30	90 30
6		0.65	-0.86	0.64	-0.86			0.26	-0.71	-0.47	-1.17
7		0.68	-0.85	0.68	-0.87			0.36	-0.67	-0.76	-1.19
8		0.68	-0.86	0.68	-0.87			0.36	-0.68	-0.72	-1.17
9		0.68	-0.88	0.66	-0.90			0.19	-0.68	-0.74	-1.19
10		0.65	-0.86	0.66	-0.87			0.04	-0.68	-0.82	-1.20
11		0.70	-0.86	0.68	-0.86			0.47	-0.64	-1.00	-1.08
12		0.62	-0.89	0.62	-0.85			0.69	-0.65	-1.17	-1.02
13		0.66	-0.89	0.65	-0.89			0.72	-0.65	-1.13	-0.95
14		0.69	-0.86	0.68	-0.87			0.33	-0.66	-1.08	-0.94
15		0.66	-0.89	0.64	-0.90			0.26	-0.67	-1.11	-0.92
16		0.62	-0.85	0.60	-0.86			0.70	-0.64	-1.13	-0.79
17		0.21	-0.88	0.21	-0.85			0.75	-0.64	-1.25	-0.79
18		0.44	-0.85	0.40	-0.87			0.85	-0.64	-1.20	-0.76
19		-0.49	-0.89	-0.53	-0.89			1.03	-0.78	-0.84	-0.82
20		-1.03	-0.83	-1.03	-0.86			0.85	-1.20	-0.07	-0.70
21		-1.42	-0.96	-1.35	-0.90			0.88	-0.49	0.75	-0.64
F 1		-0.82	-0.83	-0.87	-0.87			-0.80	-0.77	-0.65	0.93
2		-0.82	-0.83	-0.87	-0.87			-0.83	-0.74	-0.66	0.93
3		-0.82	-0.86	-0.80	-0.86			-0.86	-0.77	-0.67	0.81
4		0.60	-0.85	0.60	-0.86			0.25	-0.71	-0.33	-1.13
5		0.73	-0.88	0.74	-0.86			0.37	-0.73	-0.39	-1.17
6		0.75	-0.85	0.75	-0.87			0.29	-0.73	-0.45	-1.17
7		0.72	-0.91	0.72	-0.87			0.40	-0.70	-0.72	-1.16

TABLE 1 - Continued

Tap No.	Azimuth Angle U_o - ft/sec	180 30	0 30	180 50	0 50	45 30	135 30	225 30	315 30	270 30	90 30
8		0.71	-0.89	0.71	-0.87			0.22	-0.73	-0.73	-1.19
9		0.64	-0.89	0.66	-0.90			0.47	-0.68	-1.05	-1.05
10		0.60	-0.91	0.62	-0.89			0.53	-0.67	-1.08	-0.97
11		0.59	-0.89	0.59	-0.87			0.47	-0.67	-1.05	-0.95
12		0.79	-0.89	0.80	-0.87			0.80	-0.68	-1.09	-0.81
13		0.23	-0.89	0.20	-0.87			0.74	-0.70	-1.23	-0.78
14		-1.32	-0.86	-1.32	-0.87			0.50	-0.74	-1.22	-0.71
15		-1.09	-0.86	-1.04	-0.86			0.20	-0.29	0.82	-0.64
G 1		0.82	-0.89	0.84	-0.87	-0.80	0.35	0.54	-0.68	-1.02	-1.05
2		0.79	-0.88	0.81	-0.86	-0.80	0.22	0.60	-0.67	-1.11	-0.95
3		0.70	-0.86	0.71	-0.86	-0.80	0.17	0.87	-0.65	-1.11	-0.85
4		0.55	-0.89	0.57	-0.86	-0.79	0.14	0.73	-0.65	-1.13	-0.73
5		-1.70	-0.91	-1.77	-0.86	-0.82	-0.80	0.97	-0.83	-0.89	-0.79
6		-0.64	-0.89	-0.68	-0.88	-0.80	-0.83	0.79	-1.32	-0.81	-0.68
7		-0.82	-0.86	-0.87	-0.87	-0.85	-0.83	0.28	0.04	0.73	-0.62
8		-0.85	-0.85	-0.85	-0.86	-0.82	-0.83	0.29	0.44	0.73	-0.56
9		-0.79	-0.82	-0.81	-0.84	-0.79	-0.79	0.25	0.23	0.92	-0.55
H 1		0.90	-0.86	0.89	-0.86	-0.80	0.53	0.60	-0.71	-1.05	-1.05
2		0.83	-0.91	0.81	-0.89	-0.80	0.15	0.82	-0.71	-1.08	-0.95
3		0.86	-0.89	0.84	-0.88	-0.80	0.16	0.82	-0.71	-1.09	-0.95
4		0.89	-0.89	0.88	-0.86	-0.80	0.35	0.74	-0.68	-1.06	-0.95
5		0.91	-0.86	0.89	-0.87	-0.80	0.47	0.63	-0.71	-1.08	-0.97

TABLE 1 - Continued

Tap	Azimuth Angle	180	0	180	0	45	135	225	315	270	90
No.	U_o - ft/sec	30	30	50	50	30	30	30	30	30	30
6		0.89	-0.85	0.89	-0.89	-0.80	0.64	0.60	-0.70	-1.06	-1.00
7		0.64	-0.88	0.62	-0.88	-0.83	0.08	1.02	-0.68	-1.06	-0.76
8		-0.88	-0.86	-0.89	-0.89	-0.80	-0.82	0.26	0.75	0.95	-0.54
9		-0.88	-0.89	-0.87	-0.88	-0.80	-0.80	0.24	0.50	0.95	-0.51
10		-0.88	-0.86	-0.87	-0.89	-0.80	-0.82	0.22	0.25	0.95	-0.50
11		-0.85	-0.86	-0.86	-0.87	-0.82	-0.80	0.29	0.19	0.95	-0.50
12		-0.85	-0.85	-0.87	-0.90	-0.82	-0.80	0.52	0.22	0.95	-0.51
13		-0.85	-0.86	-0.86	-0.91	-0.82	-0.80	0.73	0.24	0.95	-0.53
J 1		0.94	-0.85	0.95	-0.81	-0.80	0.40	0.54	-0.73	-1.02	-1.06
2		0.91	-0.80	0.92	-0.79	-0.79	0.31	0.75	-0.71	-1.05	-1.00
3		0.91	-0.82	0.92	-0.81	-0.77	0.30	0.63	-0.71	-1.03	-0.98
4		0.91	-0.83	0.93	-0.77	-0.79	0.32	0.62	-0.71	-1.03	-0.98
5		0.91	-0.80	0.94	-0.86	-0.80	0.36	0.61	-0.68	-1.03	-1.00
6		0.91	-0.86	0.93	-0.84	-0.80	0.50	0.62	-0.68	-1.01	-1.03
7		0.86	-0.86	0.85	-0.85	-0.79	0.16	0.71	-0.68	-1.05	-0.90
8		0.72	-0.86	0.71	-0.84	-0.82	-0.06	0.92	-0.68	-1.06	-0.83
9		0.72	-0.86	0.70	-0.85	-0.80	-0.05	0.78	-0.68	-1.06	-0.79
10		0.72	-0.83	0.70	-0.84	-0.79	-0.04	0.79	-0.68	-1.05	-0.79
11		0.74	-0.83	0.72	-0.84	-0.80	-0.01	0.77	-0.67	-1.05	-0.79
12		0.80	-0.85	0.79	-0.81	-0.80	0.11	0.78	-0.68	-1.03	-0.81
13		0.39	-0.80	0.36	-0.86	-0.85	-0.48	0.90	-0.68	-1.05	-0.66
14		-1.53	-0.86	-1.58	-0.85	-0.83	-0.97	1.05	-0.68	-0.84	-0.66
15		-0.76	-0.83	-0.81	-0.82	-0.80	-0.79	0.81	-0.73	-1.09	-0.59

TABLE 1 - Continued

Tap No.	Azimuth Angle U_o - ft/sec	180 30	0 30	180 50	0 50	45 30	135 30	225 30	315 30	270 30	90 30
16		-0.83	-0.83	-0.87	-0.86	-0.77	-0.79	0.40	-0.34	0.73	-0.54
17		-0.85	-0.80	-0.85	-0.87	-0.80	-0.79	0.50	0.25	0.92	-0.51
18		-0.85	-0.83	-0.85	-0.80	-0.76	-0.77	0.53	0.15	0.98	-0.53
19		-0.83	-0.86	-0.84	-0.82	-0.77	-0.74	0.56	0.11	0.97	-0.53
20		-0.82	-0.80	-0.84	-0.86	-0.77	-0.77	0.59	0.08	0.97	-0.54
21		-0.83	-0.79	-0.81	-0.85	-0.77	-0.77	0.67	0.04	0.95	-0.55
22		-0.83	-0.82	-0.84	-0.82	-0.77	-0.74	0.23	0.19	0.98	-0.52
K 1		0.91	-0.74	0.90	-0.75	-0.77	0.20	0.71	-0.68	-1.02	-0.86
2		0.26	-0.77	0.24	-0.77	-0.82	-0.56	0.96	-0.68	-1.05	-0.64
3		-1.33	-0.83	-1.23	-0.84	-0.80	-0.96	1.03	-0.68	-0.85	-0.57
4		-0.70	-0.83	-0.75	-0.79	-0.77	-0.73	0.83	-0.76	-1.09	-0.53
5		-0.80	-0.85	-0.81	-0.82	-0.73	-0.72	0.42	-0.36	0.68	-0.49
6		-0.80	-0.80	-0.81	-0.77	-0.73	-0.73	0.19	0.05	0.95	-0.49
L 1		0.99	-0.73	0.99	-0.75	-0.71	0.46	0.53	-0.65	-1.00	-1.05
2		0.96	-0.71	0.97	-0.73	-0.71	0.32	0.70	-0.65	-1.03	-0.97
3		0.96	-0.70	0.97	-0.71	-0.71	0.31	0.62	-0.64	-1.02	-0.93
4		0.96	-0.76	0.97	-0.68	-0.71	0.32	0.61	-0.64	-1.00	-0.95
5		0.96	-0.74	0.97	-0.74	-0.73	0.33	0.60	-0.64	-1.02	-0.98
6		0.96	-0.73	0.97	-0.69	-0.71	0.52	0.61	-0.62	-0.98	-0.98
7		0.90	-0.73	0.88	-0.73	-0.73	0.16	0.71	-0.62	-1.02	-0.80
8		0.75	-0.73	0.72	-0.73	-0.73	-0.06	0.87	-0.62	-1.02	-0.75
9		0.74	-0.76	0.71	-0.71	-0.74	-0.08	0.79	-0.62	-1.02	-0.73

TABLE 1 - Continued

Tap No.	Azimuth Angle U_o - ft/sec	180 30	0 30	180 50	0 50	45 30	135 30	225 30	315 30	270 30	90 30
10		0.74	-0.74	0.72	-0.71	-0.73	-0.04	0.79	-0.62	-1.03	-0.68
11		0.76	-0.71	0.73	-0.69	-0.74	-0.03	0.78	-0.62	-1.00	-0.69
12		0.83	-0.73	0.81	-0.71	-0.74	0.23	0.78	-0.62	-1.02	-0.69
13		0.29	-0.74	0.26	-0.69	-0.77	-0.49	0.91	-0.62	-1.03	-0.57
14		-1.61	-0.76	-1.76	-0.79	-0.73	-0.85	1.03	-0.62	-0.87	-0.56
15		-0.64	-0.79	-0.66	-0.78	-0.70	-0.70	0.85	-0.70	-1.17	-0.50
16		-0.52	-0.79	-0.77	-0.79	-0.68	-0.67	0.46	-0.28	0.67	-0.46
17		-0.74	-0.79	-0.75	-0.75	-0.68	-0.66	0.53	0.27	0.87	-0.47
18		-0.74	-0.77	-0.76	-0.76	-0.68	-0.68	0.54	0.05	0.92	-0.46
19		-0.74	-0.76	-0.76	-0.74	-0.68	-0.68	0.56	0.05	0.92	-0.45
20		-0.74	-0.74	-0.77	-0.77	-0.68	-0.68	0.58	0.01	0.91	-0.46
21		-0.76	-0.74	-0.77	-0.76	-0.67	-0.68	0.65	0.01	0.90	-0.48
22		-0.74	-0.77	-0.77	-0.77	-0.67	-0.68	0.22	0.19	0.94	-0.45
R 1		-0.88	-0.91	-0.88	-0.90			-0.97	-0.89	-0.71	-1.14
2		-0.85	-0.86	-0.85	-0.92			-0.94	-0.85	-0.58	-1.14
3		-0.91	-0.89	-0.87	-0.84			-0.97	-0.83	-0.58	-1.14
4		-0.91	-0.94	-0.90	-0.89			-0.96	-0.85	-0.70	-1.16
5		-0.88	-0.86	-0.90	-0.91			-1.20	-0.89	-1.09	-0.98
6		-0.88	-0.89	-0.86	-0.88			-1.03	-1.02	-1.02	-1.11
7		-0.88	-0.94	-0.87	-0.90			-1.14	-0.85	-1.09	-1.03
8		-0.88	-0.86	-0.87	-0.89			-0.92	-0.85	-0.47	-1.11
9		-0.88	-0.82	-0.89	-0.95			-0.92	-0.83	-0.48	-1.11
10		-0.88	-0.88	-0.89	-0.97			-1.18	-0.61	-1.05	-1.00

TABLE 1 - Continued

Tap No.	Azimuth Angle U_o - ft/sec	180	0	180	0	45	135	225	315	270	90
		30	30	50	50	30	30	30	30	30	30
11		-0.82	-0.82	-0.82	-0.89			-1.11	-0.83	-0.95	-0.53
12		-0.88	-0.85	-0.87	-0.90			-0.83	-0.79	-0.53	-0.88
13		-0.91	-0.91	-0.89	-0.92			-0.83	-0.80	-0.55	-1.23
14		-0.88	-0.85	-0.88	-0.89			-0.85	-0.76	-0.54	-1.11
15		-0.85	-0.86	-0.88	-0.87			-0.55	-0.73	-0.82	-1.16
16		-0.85	-0.86	-0.87	-0.92			-0.41	-0.65	-0.95	-1.03
17		-0.97	-0.86	-0.95	-0.88			-0.74	-0.71	-1.27	-0.53
18		-0.94	-0.86	-0.91	-0.91			-0.30	-0.26	-0.68	-0.51

TABLE 2
Pressure Coefficients - Uniform Flow
(1:600 scale model)

$$C_p = \frac{p - p_{ref}}{\rho U_o^2 / 2}$$

Tap No.	Azimuth Angle									
	180	0	45	135	225	315	270	90		
A	1	0.81	-0.73	-0.64	0.32	0.27	-0.58	-0.50	-0.80	
	2	-0.76	-0.71	-0.71	-0.68	0.16	0.17	0.90	-0.62	
B	1	0.89	-0.73	-0.65	0.40	0.33	-0.59	-0.56	-0.84	
	2	-0.77	-0.75	-0.72	-0.69	0.21	0.23	0.96	-0.60	
C	3	0.98	-0.73	-0.68	0.46	0.40	-0.60	-0.64	-0.84	
	4	-0.76	-0.75	-0.72	-0.70	0.24	0.26	1.00	-0.56	
D	1	1.00	-0.73	-0.68	0.49	0.43	-0.61	-0.69	-0.84	
	2	-0.76	-0.75	-0.70	-0.72	0.25	0.28	1.00	-0.54	
E	1	1.00	-0.70	-0.69	0.51	0.46	-0.61	-0.74	-0.85	
	2	-0.73	-0.73	-0.72	-0.70	0.26	0.29	1.00	-0.50	
F	3	1.00	-0.65	-0.65	0.52	0.48	-0.61	-0.74	-0.84	
	4	1.00	-0.65	-0.65	0.43	0.57	-0.62	-0.83	-0.80	
	5	0.99	-0.65	-0.66	0.33	0.65	-0.62	-0.92	-0.77	
	6	0.93	-0.66	-0.67	0.19	0.73	-0.62	-1.00	-0.71	
	7	0.80	-0.67	-0.68	0.04	0.80	-0.61	-1.05	-0.65	
	8	0.50	-0.67	-0.69	-0.19	0.92	-0.61	-1.05	-0.58	
	9	-0.73	-0.74	-0.67	-0.66	0.43	-0.11	0.74	-0.47	
	10	-0.71	-0.71	-0.67	-0.66	0.55	0.18	1.00	-0.46	
	11	-0.70	-0.70	-0.67	-0.67	0.27	0.29	1.00	-0.46	
	G	1	1.00	-0.58	-0.59	0.53	0.49	-0.61	-0.75	-0.80
		2	-0.67	-0.66	-0.59	-0.63	0.29	0.30	1.00	-0.41
H	1	1.00	-0.54	-0.55	0.53	0.51	-0.58	-0.75	-0.75	
	2	-0.62	-0.66	-0.52	-0.55	0.33	0.32	1.00	-0.37	
R	1	-0.79	-0.77	-0.57	-0.55	-0.70	-0.65	-0.63	-1.02	
	2	-0.79	-0.76	-0.71	-0.67	-0.55	-0.50	-0.97	-0.68	

TABLE 3
Pressure Coefficients - Turbulent Boundary-Layer Flow
(1:600 scale model)

$$C_p = \frac{p - p_{ref}}{\rho U^2 / 2}$$

Tap No.	Azimuth Angle Ref. Velocity	180		270		
		U	U _o	U	U _o	
A 1		0.98	0.74	-0.29	-0.21	
	2	-0.69	-0.52	0.92	0.67	
B 1		0.99	0.73	-0.29	-0.21	
	2	-0.70	-0.52	0.92	0.66	
C 3		0.99	0.70	-0.34	-0.23	
	4	-0.72	-0.52	0.96	0.66	
D 1		1.00	0.68	-0.34	-0.22	
	2	-0.77	-0.53	0.99	0.64	
E 1		1.00	0.63	-0.27	-0.16	
	2	-0.88	-0.55	1.00	0.59	
F 3		1.00	0.57	-0.20	-0.11	
	4	1.00	0.57	-0.28	-0.15	
	5	0.95	0.53	-0.38	-0.20	
	6	0.92	0.52	-0.58	-0.31	
	7	0.83	0.47	-0.83	-0.45	
	8	0.50	0.28	-1.00	-0.54	
	9	-1.18	-0.67	0.82	0.44	
	10	-1.10	-0.62	0.98	0.53	
	11	-0.96	-0.54	1.00	0.54	
	G 1		1.00	0.45	-0.18	-0.08
		2	-1.07	-0.48	1.00	0.42
H 1		1.00	0.30	-0.15	-0.03	
	2	-1.11	-0.33	1.00	0.17	
R 1		-0.52	-0.41	-0.33	-0.25	
	2	-0.54	-0.42	-0.63	-0.48	

TABLE 3 - Continued

Tap No.	Azimuth Angle	180		270	
	Ref. Velocity	U	U _o	U	U _o
C 1				-0.26	-0.18
6		-0.57	-0.41		
F 1				-0.29	-0.15
13		-0.71	-0.40		

IV. SURFACE PRESSURE-DIFFERENCE FLUCTUATIONS

The purpose of this phase of the study was to explore the effect of wind speed, direction and turbulence on pressure-difference fluctuations at selected points on the 1:200 scale model. Since the local flow instabilities produced by the building geometry are a basic source of these fluctuations, the model was placed in a uniform air stream and the critical azimuth angles for the selected points were determined for velocities of 30 and 50 ft/sec.

Peak values of the pressure-difference fluctuations occurred in very narrow ranges of azimuth angle and the critical angles were in most cases independent of velocity. Once the critical angle for a set of taps had been determined, the signal was observed on an oscilloscope for about 30 sec. to determine the peak fluctuation. The signal was then repeatedly stored and rejected until this maximum appeared in a sample which was then photographed for further analysis. RMS values of these pressure-difference fluctuations were also recorded.

A similar procedure was followed in determining the contribution of turbulence in the approach flow. For this part of the study the 1:200 scale model was placed in a turbulent boundary-layer flow. As it was not possible to submerge the entire height of the 1:200 scale model in a boundary layer, only those tap combinations at or below "J" level were investigated for contributions due to turbulence in the approach flow. Although the critical wind directions were not as clearly defined for the turbulent case they were found to be in good agreement with those for the uniform flow case.

These data are presented in Tables 4 and 5. The column titled

$\frac{\Delta p'_{\max}}{\rho U_o^2/2}$ is the ratio of one-half the peak to peak fluctuation to the

dynamic head of the approach flow. These values divided by

$\frac{\Delta p'_{rms}}{\rho U_o^2 / 2}$ give the number of standard deviations between the mean

and the maximum peak assuming a normal distribution. The local mean velocity U was used for the boundary-layer flow case. The distribution of instantaneous maximum values for a given set of pressure taps was not determined. The frequencies of these fluctuations ranged from 30 to 70 cycles/sec. A typical trace of the transducer output is reproduced in Fig. 20.

Velocity distributions and turbulence intensities for the boundary-layer flows at three stations upstream of the BAWHB are presented in Table 6.

For this phase of the study, the 1:200 scale model was modified to account for architectural revisions made after the original model was constructed. The interchanging of the east and west sides of the model should have no effect on the results obtained.

TABLE 4
Surface Pressure-Difference Fluctuations
(Uniform Flow)

Tap Combination	Azimuth Angle	Δh_o (mm Hg.)	$\frac{\Delta p'_{\max}}{\rho U_o^2 / 2}$	$\frac{\Delta p'_{\text{rms}}}{\rho U_o^2 / 2}$	$\frac{\Delta p'_{\max}}{\sigma}$
E8-7	114	0.282	0.495	0.156	3.17
E8-7	114	0.800	0.650	0.165	3.94
E8-7	236	0.395	0.810	0.258	3.14
E8-7	236	0.800	0.710	0.270	2.63
E15-14	121	0.305	0.690	0.184	3.75
E15-14	123	0.735	0.610	0.196	3.11
E18-17	235	0.360	0.695	0.250	2.78
E18-17	237	0.778	0.760	0.208	3.65
F5-4	260	0.330	0.820	0.303	2.71
F5-4	260	0.795	1.01	0.316	3.20
G8-7	219	0.337	0.740	0.184	4.02
G8-7	219	0.802	0.995	0.239	4.16
G8-7	331	0.330	0.940	0.351	2.68
G8-7	331	0.802	0.725	0.316	2.29
H3-2	243	0.385	0.650	0.218	2.98
H3-2	243	0.805	0.620	0.209	2.97
H6-5	140	0.330	0.455	0.145	3.14
H6-5	140	0.785	0.395	0.132	2.99
H6-5	228	0.325	0.370	0.142	2.61
H6-5	228	0.790	0.430	0.152	2.83
H6-5	243	0.280	0.570	0.164	3.48
H6-5	243	0.800	0.550	0.155	3.55
H13-12	214	0.377	0.715	0.234	3.06
H13-12	212	0.805	0.790	0.244	3.24
J3-2	98	0.380	0.343	0.074	4.64
J3-2	98	0.840	0.238	0.067	3.55
J3-2	247	0.345	0.233	0.104	2.24
J3-2	247	0.825	0.340	0.092	3.70
J6-5	98	0.320	0.313	0.094	3.33
J6-5	98	0.675	0.370	0.086	4.30
J9-8	90	0.300	0.200	0.067	2.99
J9-8	250	0.295	0.272	0.104	2.62
J9-8	250	0.745	0.201	0.062	3.24
J12-11	106	0.330	0.425	0.133	3.20
J12-11	106	0.745	0.309	0.113	2.74
J18-17	341	0.340	0.530	0.165	3.21
J18-17	341	0.680	0.471	0.156	3.02
J21-20	209	0.310	0.404	0.142	2.85

TABLE 4 - Continued

Tap Combination	Azimuth Angle	Δh_o (mm Hg.)	$\frac{\Delta p'_{\max}}{\rho U_o^2/2}$	$\frac{\Delta p'_{\text{rms}}}{\rho U_o^2/2}$	$\frac{\Delta p'_{\max}}{\sigma}$
J21-20	209	0.580	0.397	0.117	3.39
J21-20	314	0.325	0.185	0.080	2.31
J21-20	314	0.585	0.274	0.075	3.65
L3-2	98	0.380	0.421	0.079	5.33
L3-2	98	0.840	0.310	0.064	4.84
L3-2	247	0.345	0.280	0.093	3.01
L3-2	247	0.825	0.267	0.080	3.34
L6-5	98	0.320	0.530	0.150	3.53
L6-5	98	0.675	0.475	0.137	3.47
L9-8	90	0.300	0.234	0.067	3.49
L9-8	250	0.295	0.407	0.122	3.34
L9-8	250	0.745	0.299	0.118	2.53
L12-11	106	0.330	0.455	0.138	3.30
L12-11	106	0.745	0.430	0.118	3.64
L18-17	341	0.340	0.590	0.171	3.45
L18-17	341	0.680	0.588	0.150	3.92
L21-20	209	0.310	0.452	0.135	3.35
L21-20	209	0.580	0.345	0.131	2.63
L21-20	314	0.325	0.154	0.037	4.16

TABLE 5
Surface Pressure-Difference Fluctuations
(Turbulent Boundary-Layer Flow)

Tap Combination	Azimuth Angle	Δh (mm Hg.)	$\frac{\Delta p'_{\max}}{\rho U^2/2}$	$\frac{\Delta p'_{\text{rms}}}{\rho U^2/2}$	$\frac{\Delta p'_{\max}}{\sigma}$	Direction Tested
J3-2	98	0.263	0.532	0.091	5.85	W
J3-2	99	0.348	0.316	0.080	3.95	S
J3-2	90	0.940	0.278	0.072	3.86	S
J3-2	98	0.940	0.298	0.089	3.35	S
J3-2	98	0.686	0.408	0.093	4.39	W
J3-2	248.5	0.282	0.610	0.142	4.30	SW
J3-2	249	0.263	0.380	0.122	3.12	W
J3-2	225	0.792	0.253	0.086	2.94	SW
J3-2	247	0.686	0.364	0.134	2.72	W
J3-2	250	0.792	0.606	0.142	4.27	SW
J6-5	90	0.348	0.460	0.104	4.42	S
J6-5	99	0.263	0.646	0.106	6.09	W
J6-5	95	0.940	0.436	0.106	4.11	S
J6-5	101	0.686	0.495	0.122	4.06	W
J6-5	168	0.940	0.149	0.043	3.47	S
J9-8	96	0.263	0.456	0.091	5.01	W
J9-8	98	0.348	0.288	0.092	3.13	S
J9-8	90	0.940	0.383	0.094	4.07	S
J9-8	98	0.686	0.481	0.093	5.17	W
J9-8	154	0.348	0.259	0.069	2.66	S
J9-8	257	0.263	0.532	0.122	4.36	W
J9-8	180	0.940	0.149	0.028	5.32	S
J9-8	253	0.686	0.510	0.157	3.25	W
J12-11	98	0.348	0.517	0.161	3.21	S
J12-11	100	0.263	0.874	0.183	4.78	W
J12-11	98	0.940	0.639	0.145	4.41	S
J12-11	102	0.686	0.875	0.192	4.56	W
J12-11	180	0.940	0.213	0.053	4.02	S
J18-17	342	0.263	0.532	0.198	2.69	W
J18-17	333	0.686	0.554	0.198	2.80	W
J21-20	202	0.282	0.683	0.113	5.65	SW
J21-20	225	0.282	0.426	0.099	4.30	SW
J21-20	205	0.792	0.732	0.141	5.19	SW
J21-20	225	0.792	0.354	0.091	3.89	SW
J21-20	343	0.263	0.608	0.106	5.74	W
J21-20	341	0.686	0.437	0.117	3.74	W
L3-2	98	0.196	0.408	0.102	4.00	W
L3-2	99	0.290	0.483	0.069	7.00	S

TABLE 5 - Continued

Tap Combination	Azimuth Angle	Δh (mm Hg.)	$\frac{\Delta p'_{\max}}{\rho U^2/2}$	$\frac{\Delta p'_{\text{rms}}}{\rho U^2/2}$	$\frac{\Delta p'_{\max}}{\sigma}$	Direction Tested
L3-2	90	0.789	0.228	0.091	2.51	S
L3-2	98	0.485	0.412	0.099	4.16	W
L3-2	98	0.789	0.253	0.066	3.83	S
L3-2	248.5	0.228	0.526	0.158	3.33	SW
L3-2	249	0.196	0.408	0.143	2.85	W
L3-2	225	0.652	0.368	0.098	3.76	SW
L3-2	255	0.652	0.506	0.160	3.16	SW
L3-2	255	0.485	0.454	0.173	2.62	W
L6-5	90	0.290	0.690	0.207	3.33	S
L6-5	99	0.196	0.918	0.184	4.99	W
L6-5	90	0.789	0.811	0.195	4.16	S
L6-5	99	0.485	0.928	0.198	4.69	W
L6-5	168	0.789	0.140	0.051	2.75	S
L9-8	96	0.196	0.765	0.102	7.50	W
L9-8	98	0.290	0.276	0.069	4.00	S
L9-8	96	0.789	0.456	0.066	6.91	S
L9-8	98	0.485	0.495	0.115	4.30	W
L9-8	257	0.196	0.612	0.224	2.73	W
L9-8	180	0.789	0.304	0.033	9.21	S
L9-8	253	0.485	0.866	0.248	3.49	W
L9-8	266	0.485	1.38	0.248	5.57	W
L12-11	98	0.290	0.828	0.179	4.63	S
L12-11	100	0.196	0.816	0.245	3.33	W
L12-11	92	0.789	0.621	0.178	3.49	S
L12-11	103	0.485	1.07	0.248	4.32	W
L12-11	180	0.789	0.241	0.069	3.49	S
L18-17	341	0.196	1.02	0.266	3.84	W
L18-17	345	0.485	1.03	0.314	3.28	W
L21-20	202	0.228	1.05	0.193	5.46	SW
L21-20	225	0.228	0.438	0.123	3.56	SW
L21-20	204	0.652	1.24	0.221	5.61	SW
L21-20	225	0.652	0.430	0.116	3.71	SW
L21-20	343	0.196	0.612	0.143	4.28	W
L21-20	341	0.485	0.618	0.132	4.68	W

TABLE 6
Turbulence Intensities
(1:200 scale model)

San Francisco - South					
Station	y (Inches)	U_o			
		31.00 ft/sec		51.50 ft/sec	
		$\frac{U}{U_o}$	$\frac{\sqrt{\overline{u^2}}}{U_o}$	$\frac{U}{U_o}$	$\frac{\sqrt{\overline{u^2}}}{U_o}$
25	20	0.76	0.12	0.70	0.14
	30	0.95	0.07	0.94	0.09
	40	1.00	0.05	1.00	0.05
30	20	0.86	0.15	0.82	0.15
	30	1.00	0.10	0.99	0.10
	40	1.00	0.05	1.00	0.05
32 + 0.08	20	0.76	0.16	0.73	0.15
	30	0.87	0.10	0.86	0.11
	40	0.93	0.05	0.92	0.06

San Francisco - Southwest					
Station	y (Inches)	U_o			
		31.28 ft/sec		52.15 ft/sec	
		$\frac{U}{U_o}$	$\frac{\sqrt{\overline{u^2}}}{U_o}$	$\frac{U}{U_o}$	$\frac{\sqrt{\overline{u^2}}}{U_o}$
25	20	0.72	0.12	0.75	0.13
	30	0.89	0.10	0.89	0.10
	40	0.98	0.06	0.98	0.05
30	20	0.78	0.12	0.76	0.13
	30	0.89	0.09	0.89	0.10
	40	0.97	0.07	0.99	0.06
31 + 0.16	20	0.70	0.13	0.71	0.13
	30	0.83	0.12	0.81	0.11
	40	0.91	0.07	0.92	0.08

TABLE 6 - Continued

		San Francisco - West			
Station	y (Inches)	U_o			
		31.20 ft/sec		52.00 ft/sec	
		$\frac{U}{U_o}$	$\frac{\sqrt{u^2}}{U_o}$	$\frac{U}{U_o}$	$\frac{\sqrt{u^2}}{U_o}$
25	20	0.57	0.25	0.58	0.26
	30	0.87	0.13	0.90	0.12
	40	0.99	0.07	1.00	0.06
30	20	0.64	0.13	0.68	0.16
	30	0.83	0.13	0.89	0.13
	40	0.95	0.07	0.98	0.08
32 + 0.23	20	0.65	0.12	0.68	0.13
	30	0.70	0.12	0.75	0.13
	40	0.81	0.09	0.82	0.07

V. CHARACTERISTIC EDDY-SHEDDING FREQUENCIES

The shedding frequencies of large-scale eddies were investigated for two wind directions (S and W) and two wind speeds (30 and 60 ft/sec) using a 1:600 scale model submerged in a uniform air stream and in a turbulent boundary-layer flow.

First attempts at measuring these frequencies were by means of pressure transducers mounted inside the model and connected to pressure taps located on opposite sides near the downstream portion of the model. However, the long pressure lines (about 10 in.) of 1/16 in. I. D. tubing which were required due to the model construction attenuated the signal to such an extent that it could not be identified in the background noise and signals due to local pressure pulsations. Therefore, a hot-wire anemometer was used for this phase of the study.

By using two hot-wires at equal positions but on opposite sides of the model, it was possible to observe the shedding periods and phase differences. The signal traces were simultaneously stored on a dual-beam oscilloscope and photographed for later analysis. Results of this phase of the study are presented in Table 7 along with the corresponding Strouhal numbers, $S = \frac{nD}{U}$.

Shedding frequencies for the non-turbulent case with an azimuth angle of 270° were measured only with pressure transducers which gave a wide range of values for S and hence these data are not presented here. However, it is quite probable that the true values of S for this case are very close to those obtained in a turbulent boundary layer.

These values compare favorably with results obtained by Parkinson (1) for a rectangular prism having the same width to depth ratio. Results obtained by Vickery (2) for a square prism indicate the Strouhal number is largely independent of turbulence intensity.

The data for 180° indicate an increase in S of approximately 10% for turbulent flow. However, the data are somewhat scattered and a more sophisticated method; i. e., spectral analysis, would be required to verify this.

TABLE 7
Strouhal Numbers

$$S = \frac{n D}{U_o}$$

Azimuth Angle	Type of Flow	U_o or U (ft/sec)	n (cycles/sec)	D (ft)	S
180	Uniform	32.1	12.5	0.403	0.16
"	"	63.4	25.0	"	0.16
"	"	31.6	10.0	"	0.13
"	"	"	10.4	"	0.13
"	"	63.2	17.6	"	0.11
"	"	"	18.5	"	0.12
					Average = 0.14
180	Turbulent boundary-layer	25.7	11.9	0.403	0.19
"	"	"	9.8	"	0.15
"	"	"	"	"	0.15
"	"	53.7	19.2	"	0.14
"	"	"	25.0	"	0.19
"	"	56.3	17.9	"	0.13
"	"	"	16.7	"	0.12
"	"	"	"	"	0.12
					Average = 0.15
270	Turbulent boundary-layer	26.7	16.7	0.233	0.15
"	"	56.5	25.0	"	0.10
"	"	24.4	11.1	"	0.11
"	"	"	12.5	"	0.12
"	"	"	11.1	"	0.11
"	"	"	10.0	"	0.10
"	"	52.6	31.2	"	0.14
"	"	"	27.8	"	0.12
"	"	"	26.8	"	0.11
"	"	56.2	19.2	"	0.08
					Average = 0.11

VI. GENERAL FLOW PATTERNS AROUND BUILDING

Flow patterns near street level were recorded for two wind directions (S and W) and two wind speeds (30 and 60 ft/sec) using the 1:600 scale model. Small flags (yarn tufts) pivoted on pins stuck into the model provided the general wind directions. The average height of the flags above street level was 1/4 in. and they were photographed with a 35 mm camera. Exposure time was 1/20 sec. Since wind directions near the base of the building and in the plaza area were of greatest interest, it was necessary to take two pictures at slightly different angles for each combination of wind speed and direction to show the complete pattern. These pictures are reproduced in Figs. 21 and 22. The boundary-layer thickness over the site was approximately 32 in. which corresponds to a prototype boundary-layer thickness of 1600 ft. As can be seen from Figs. 21 and 22, the general flow pattern is for all purposes independent of wind speed.

Vertical profiles of wind speed were taken upstream of the structure for the two wind directions. The free-stream velocity ranged from 30 to 60 ft/sec. These profiles were taken at Sutter Street for the southerly direction and at Grant and Taylor Streets for the westerly direction and are reproduced in Figs. 23-27 along with the equation of the form $\frac{U}{U_o} = 1 + B \log \left(\frac{y}{\delta} \right)$ which best describes the velocity distribution. U is the local mean velocity at height y , U_o is the free-stream velocity, δ is the boundary-layer thickness and B is a constant.

In addition to the velocity profiles, turbulence data were also taken at these locations. The turbulence intensities are given in Table 8.

Measurements of the downflow on the windward face of the model were made with a free-stream velocity of 30 ft/sec. For the

southerly direction this downflow was 13.0 ft/sec at a point 1 in. above street level and 13.3 ft/sec at 4-1/2 in. above street level for the westerly direction. These measurements were made with a hot-wire placed in the plane of the wall apexes at the model center line.

TABLE 8
Turbulence Intensities
(1:600 scale model)

San Francisco - South

Location	y (Inches)	U_o (ft/sec)	$\frac{U}{U_o}$	$\frac{\sqrt{u^2}}{U_o}$
Sutter St.	4	30.60	0.53	0.15
"	8	"	0.73	0.13
"	12	"	0.85	0.12
"	16	"	0.91	0.10
"	20	"	0.96	0.06

San Francisco - West

Location	y (Inches)	U_o (ft/sec)	$\frac{U}{U_o}$	$\frac{\sqrt{u^2}}{U_o}$
Grant St.	4	30.20	0.50	0.25
"	8	"	0.74	0.12
"	12	"	0.83	0.11
"	16	"	0.91	0.09
"	20	"	0.96	0.05

VII. SUMMARY OF FINDINGS AND RECOMMENDATIONS

Results of this wind tunnel study of the Bank of America World Headquarters Building are summarized in the following statements.

1. The maximum negative pressure coefficient measured in this study was -1.77 which occurred on the SW corner of the BAWHB at an azimuth angle of 180° . The maximum negative pressure coefficient measured on the roof was -1.27 at an azimuth angle of 270° .
2. On the basis of tests conducted on the 1:600 scale model covered with cardboard sheets, the base pressure intensities are about 20% less for the proposed structure than would be obtained for a similar structure having smooth walls.
3. Surface pressure-difference fluctuations on the order of one dynamic pressure were obtained in a uniform flow and in a turbulent boundary-layer flow these fluctuations were as much as 1.4 times the dynamic pressure. Frequencies of these fluctuations for the 1:200 scale model ranged from 30 to 70 cycles/sec.
4. The average Strouhal numbers for turbulent boundary-layer flows were found to be 0.15 and 0.11 for azimuth angles of 180° and 270° respectively. The Strouhal number does not appear to be influenced greatly by the intensity of turbulence.
5. Flow patterns around the BAWHB at street level are independent of wind speed. An intense downflow exists on the windward face of the structure which may contribute to pedestrian discomfort.
6. Wind-speed profiles immediately upstream of the site can be approximated by the empirical expression of the form

$$\frac{U}{U_0} = 1 + B \log \left(\frac{Y}{\delta} \right) .$$

Based on the results obtained, the following general conclusions can be made.

1. Since it was impossible to fully investigate the mean pressures at the corners of the model due to interior bracing, either the magnitude of the recorded pressures should be increased in these areas or additional work should be done with a revised model.
2. This study of surface pressure-difference fluctuations was of an exploratory nature. The phenomenon which causes these fluctuations is extremely complex and additional work directed toward a better understanding of it along with methods of controlling it should be undertaken if the present results indicate the integrity of the glass panels is in doubt. Preliminary studies indicate that the surface pressure-difference intensities can be reduced by 30 to 50% with the installation of panels of proper size and shape along the wall line where the setbacks occur. These panels evidently destroy the vortex system which is directed upward along the fluted walls of the model. Aerodynamic scale effects would have to be considered in applying model results to the prototype but it is likely that the effect of these panels would be greater for the prototype than for the model.
3. Wind screens may be required near the bottom of the building to disperse the jets which flow downward along the fluted sides of the building into pedestrian areas.

REFERENCES

1. Parkinson, G. V., Aspects of the Aeroelastic Behavior of Bluff Cylinders. EIC 1962. Ann. Gen. Mtg. Paper No. 58.
2. Vickery, B. J., Fluctuating Lift and Drag on a Long Cylinder of Square Cross-Section in a Smooth and in a Turbulent Stream. J. Fluid Mech., 1966, 25, 481-94.

APPENDIX A

Equipment List

Oscilloscope	Tektronix Type 564 Storage Oscilloscope. Time Base: Type 3B3. Amplifier: Type 3A72 Dual Trace.
Camera	Tektronix Type C27 with Elgeet 3 in. f 1.9 lens. Film: Polaroid Type 46-L.
Manometer	Trans-Sonics Type 120 B Equibar Pressure Meter - Serial 44801 - Differential Capacitance. D. C. Output: 0-30 millivolts $\pm 2\%$, proportional to pressure. Accuracy of meter reading: $\pm 3\%$ full scale of selected range. Response time: 10 milliseconds to 63% of a step change in pressure at atmospheric pressure. Range: 0.001 mm Hg. to 3 mm Hg. full scale in 7 steps.
Amplifiers	Model 112A Cohu Wideband D. C. Amplifier. Gain: 1000 Max. in 10 steps. Gain accuracy: $\pm 0.01\%$ Input impedance: 100,000 ohms. Output impedance: less than 1 ohm. Noise: Less than 5 microvolts RMS at 0 to 750 cps. Linearity: Better than 0.05% to 1 kc. Frequency response: $\pm 0.5\%$ to 2 kc. Rise time: Less than 10 microseconds to within 1%.
RMS Meter	Bruel and Kjaer Type 2416 Electronic Voltmeter. Range: 10 millivolts to 1000 volts full scale deflec- tion in 10 db steps. Frequency response: Linear to

APPENDIX A - Continued

within ± 0.02 db RMS from 2 cps to 200,000 cps.
Input impedance: 10M ohms,
Output impedance: 50 ohms,
Noise: Less than 100 microvolts at input terminals.

Pressure
Transducers

Statham Model PM283 Pressure Transducer.
Range: ± 0.15 psid.
Full scale output: Approx. ± 20 millivolts @ 5
volts.
Approx. natural frequency: 2000 cps.
Acceleration response - % FS/g:
1.1 for 0-500 cps.
1.0 for static.

X-Y Plotter

Moseley Autograph Model 135C X-Y Recorder
Input resistance: 200,000 ohms/volt full scale.
Accuracy: $\pm 0.1\%$ of full scale.
Slewing speed: 15 inches per second each axis.

Anemometer

Model HW 300B Constant Temperature Hot-Wire
Anemometer.
Frequency response: Flat to 80 kc.

FIGURES

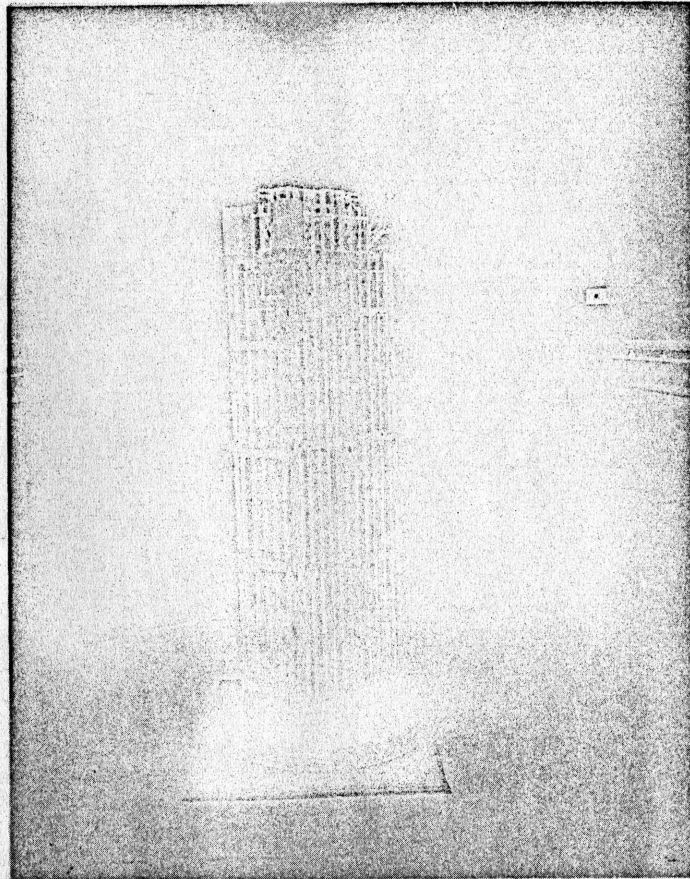


Fig. 1 1:200 Scale Model



Fig. 2 1:600 Scale Model

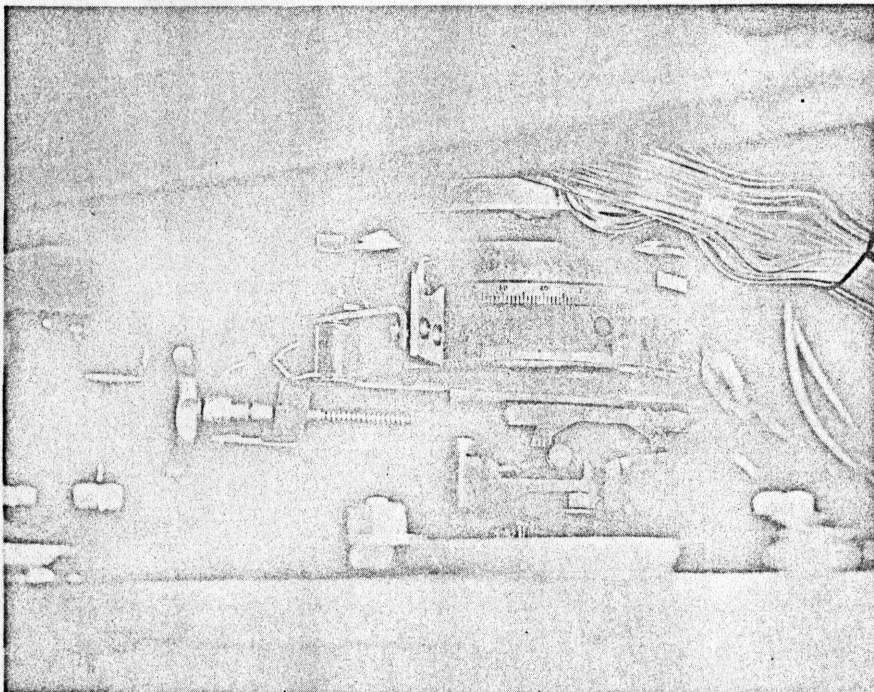


Fig. 3 Rotary Table

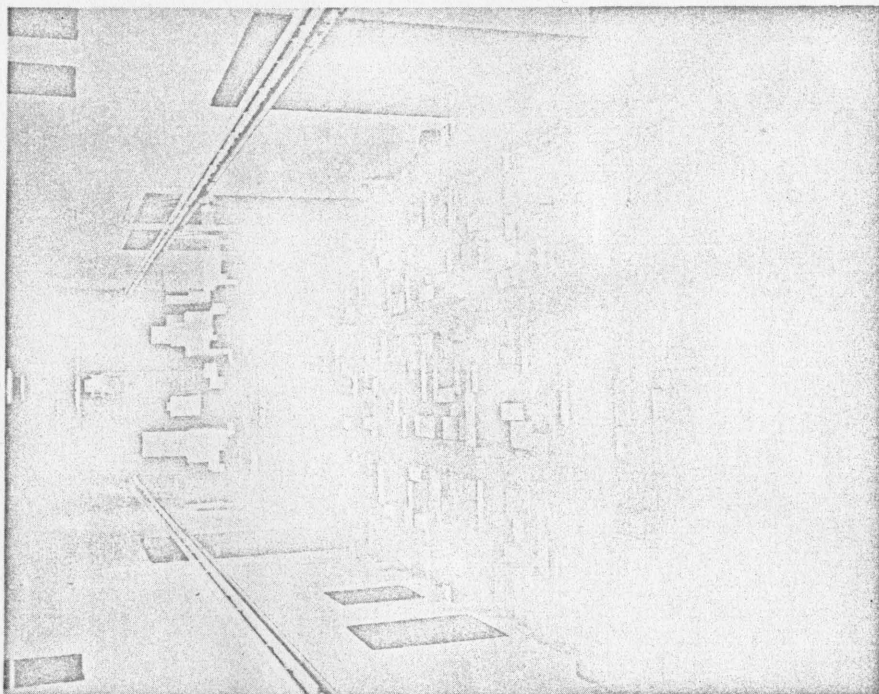


Fig. 5 S. F. West
Scale = 1:200



Fig. 4 S. F. Southwest
Scale = 1:200

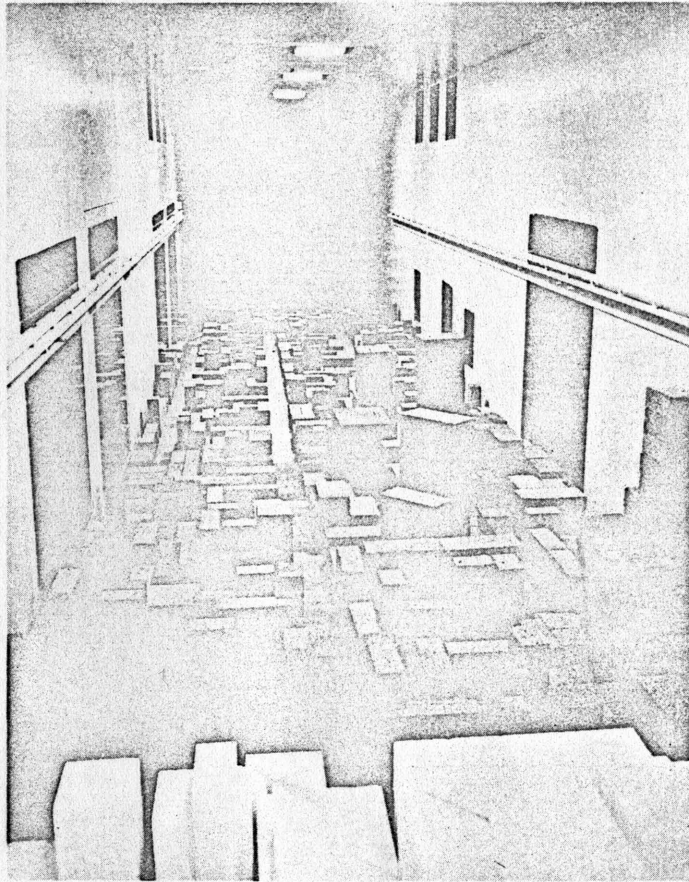


Fig. 6 S. F. West (Looking upstream)
Scale = 1:200

Fig. 7 Low-Speed Wind Tunnel

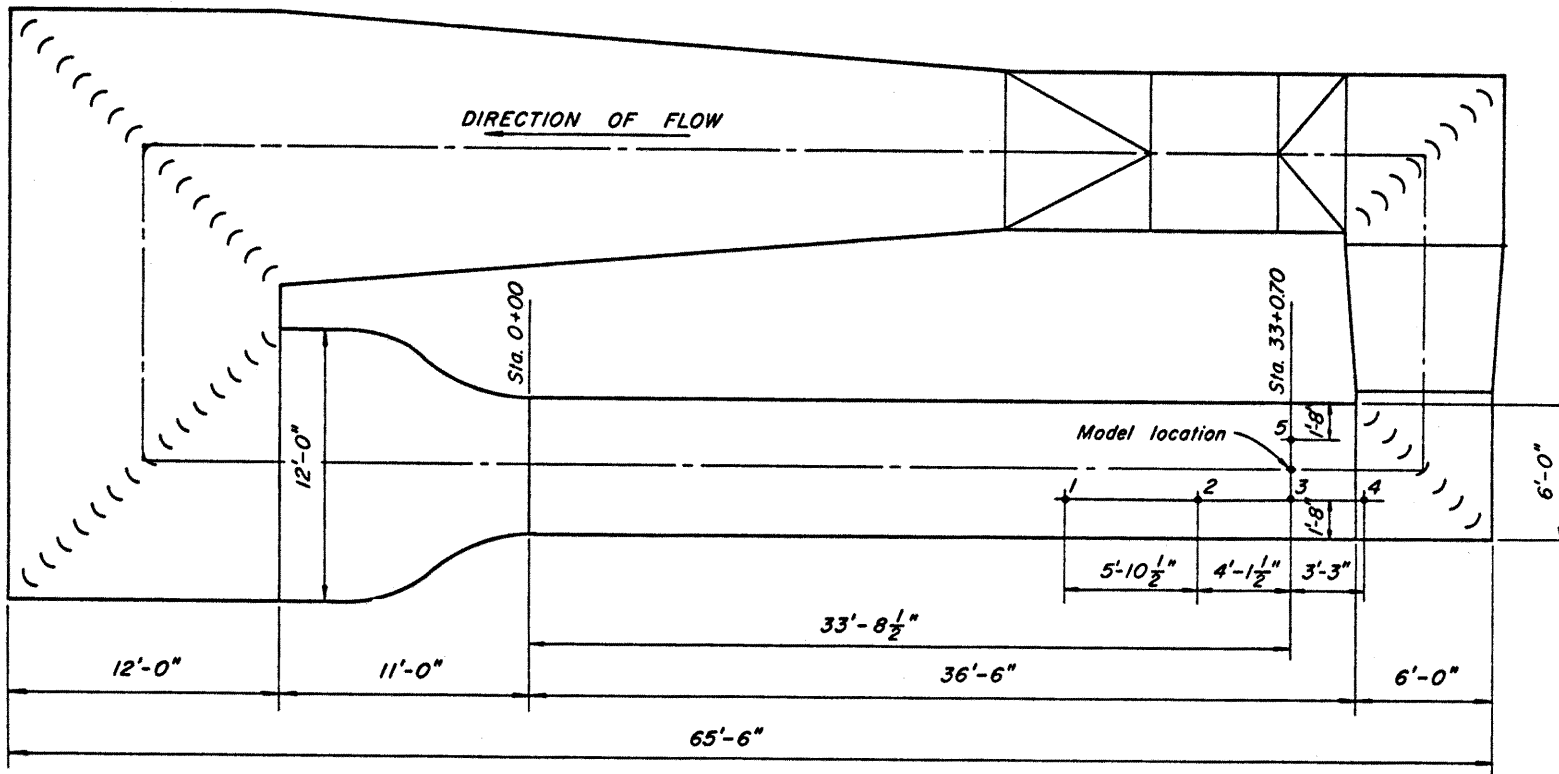


Fig. 7 - Low-Speed Wind Tunnel

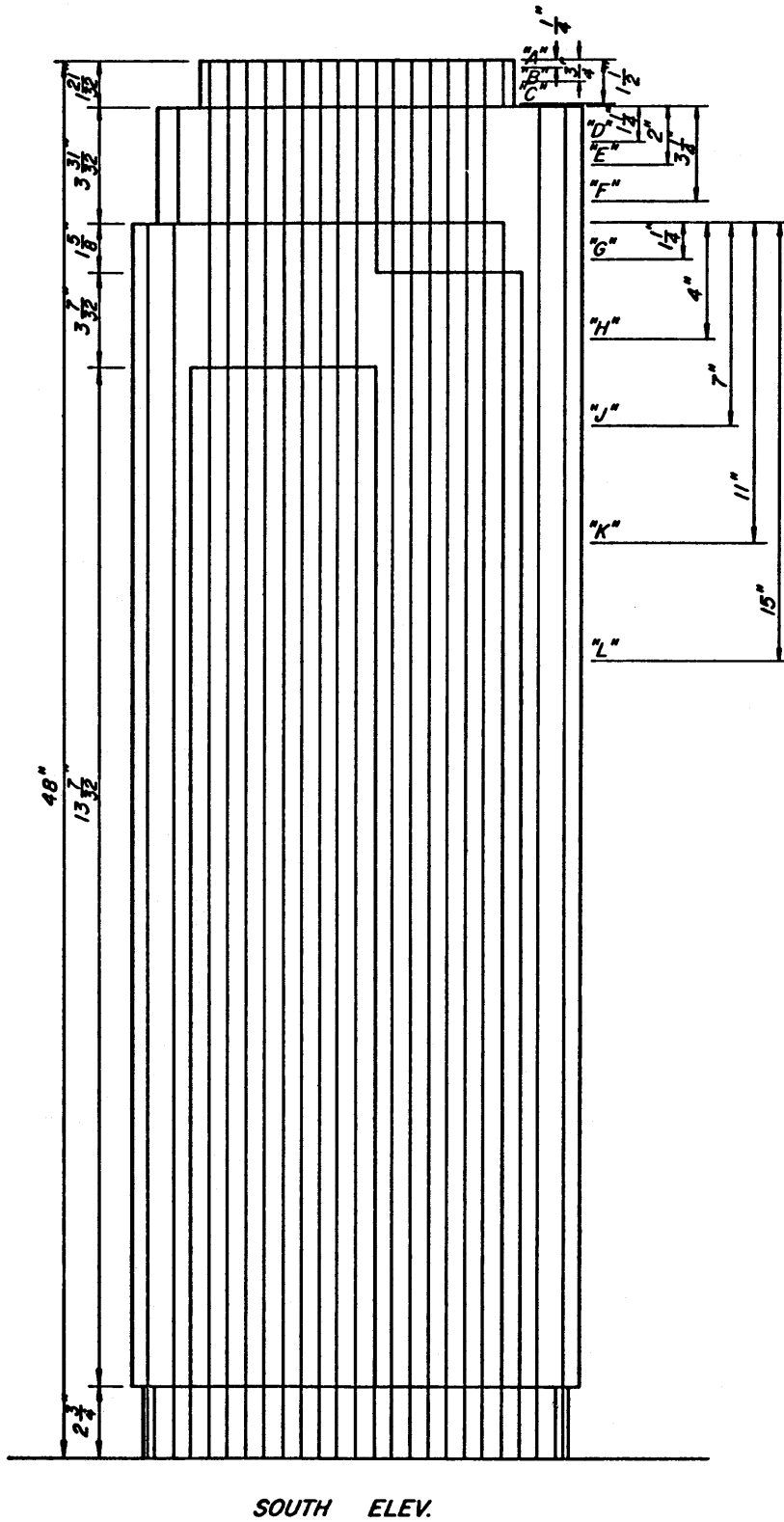


Fig. 8 Pressure Tap Arrangement
(1:200 Scale Model)

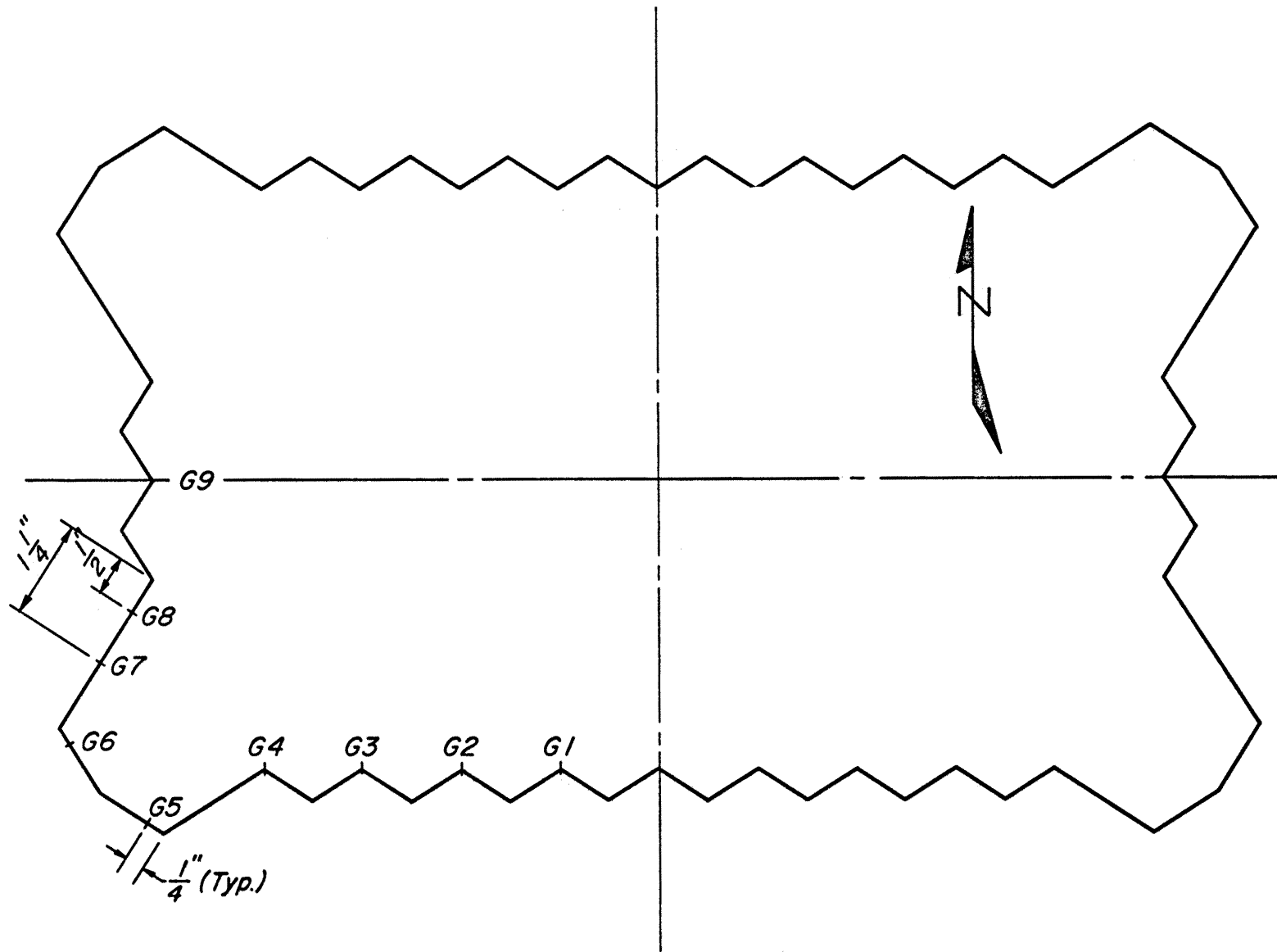


Fig. 10 - Pressure Tap Arrangement
Level G
(1/2 scale)

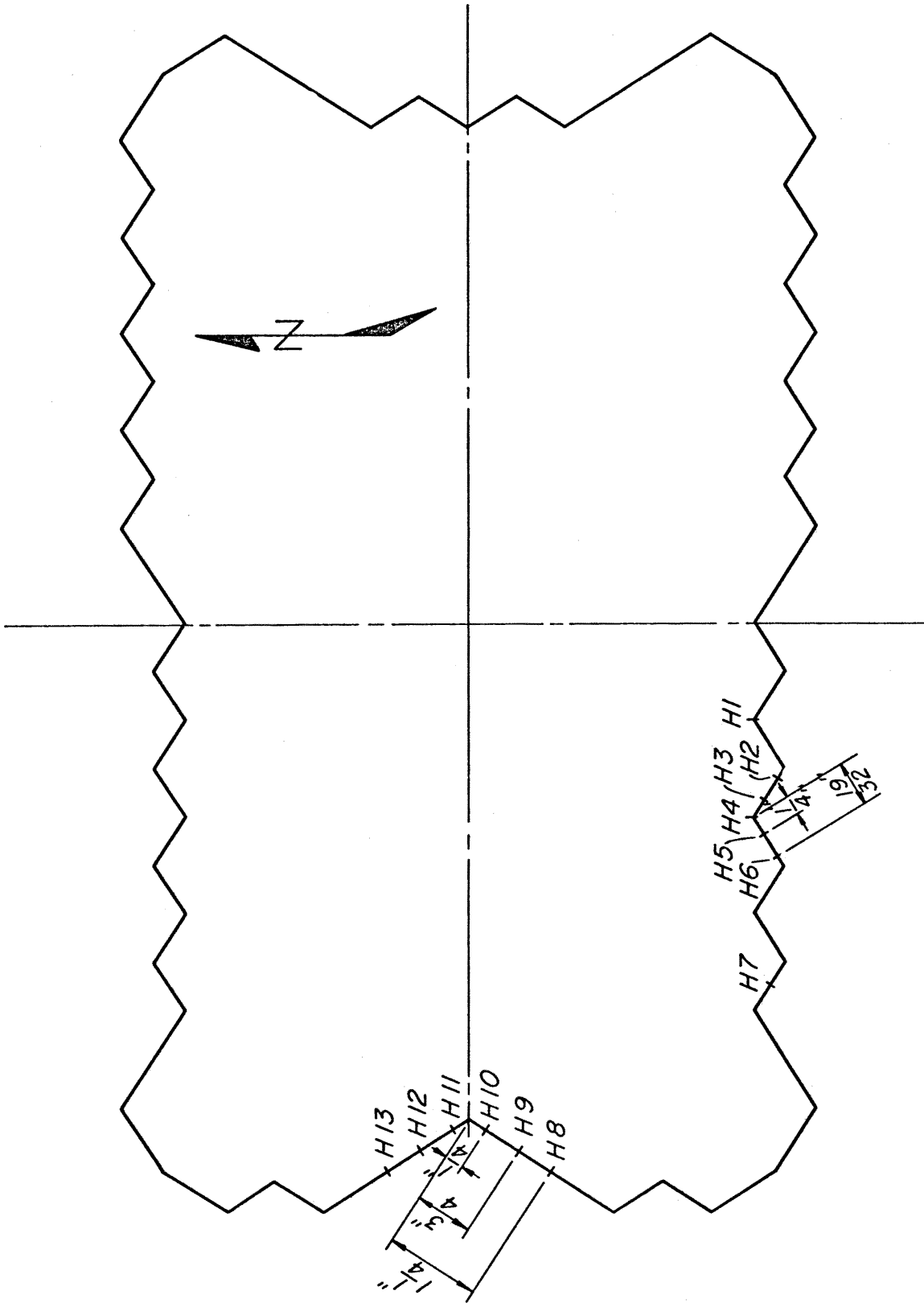


Fig. 11 - Pressure Tap Arrangement
Level H
(1/2 scale)

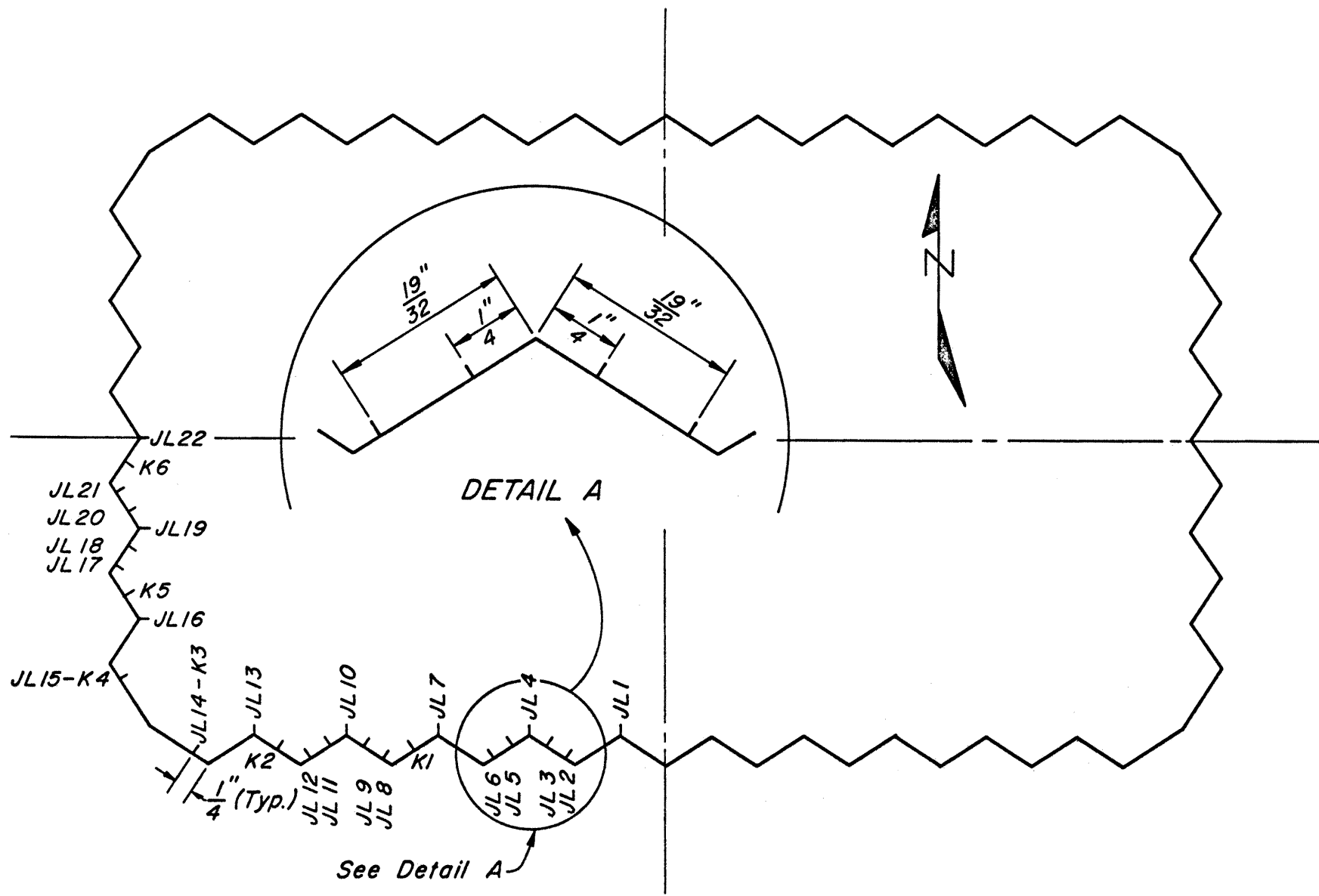


Fig. 12 - Pressure Tap Arrangement
 Levels J, K & L
 (1/2 scale)

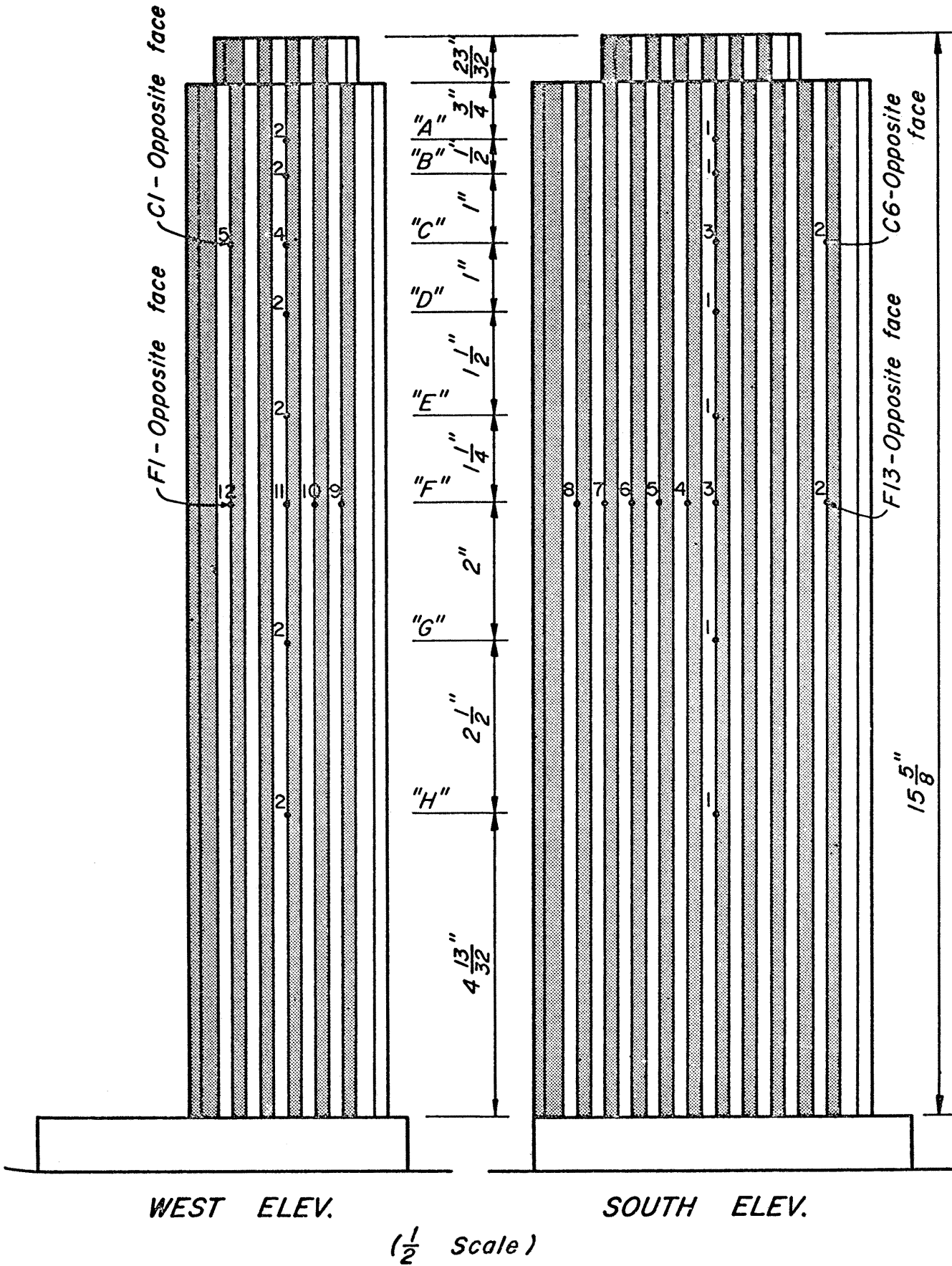


Fig. 13 - Pressure Tap Arrangement (1:600 Scale Model)

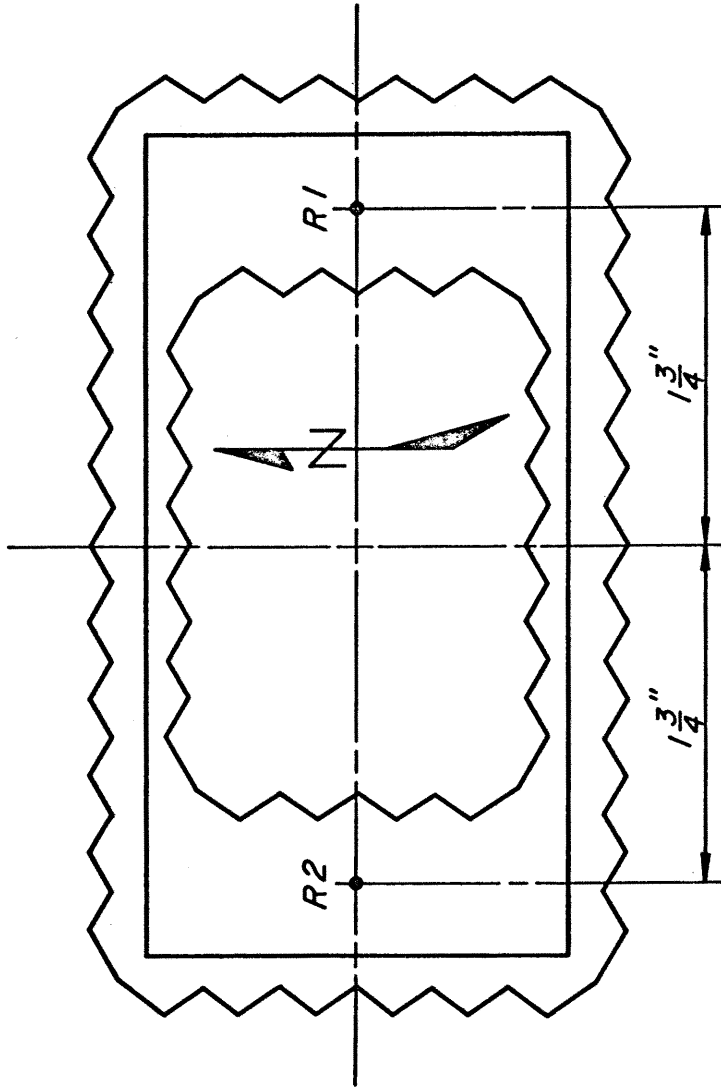


Fig. 14 Roof Plan - 1:600 Scale Model (To Scale)

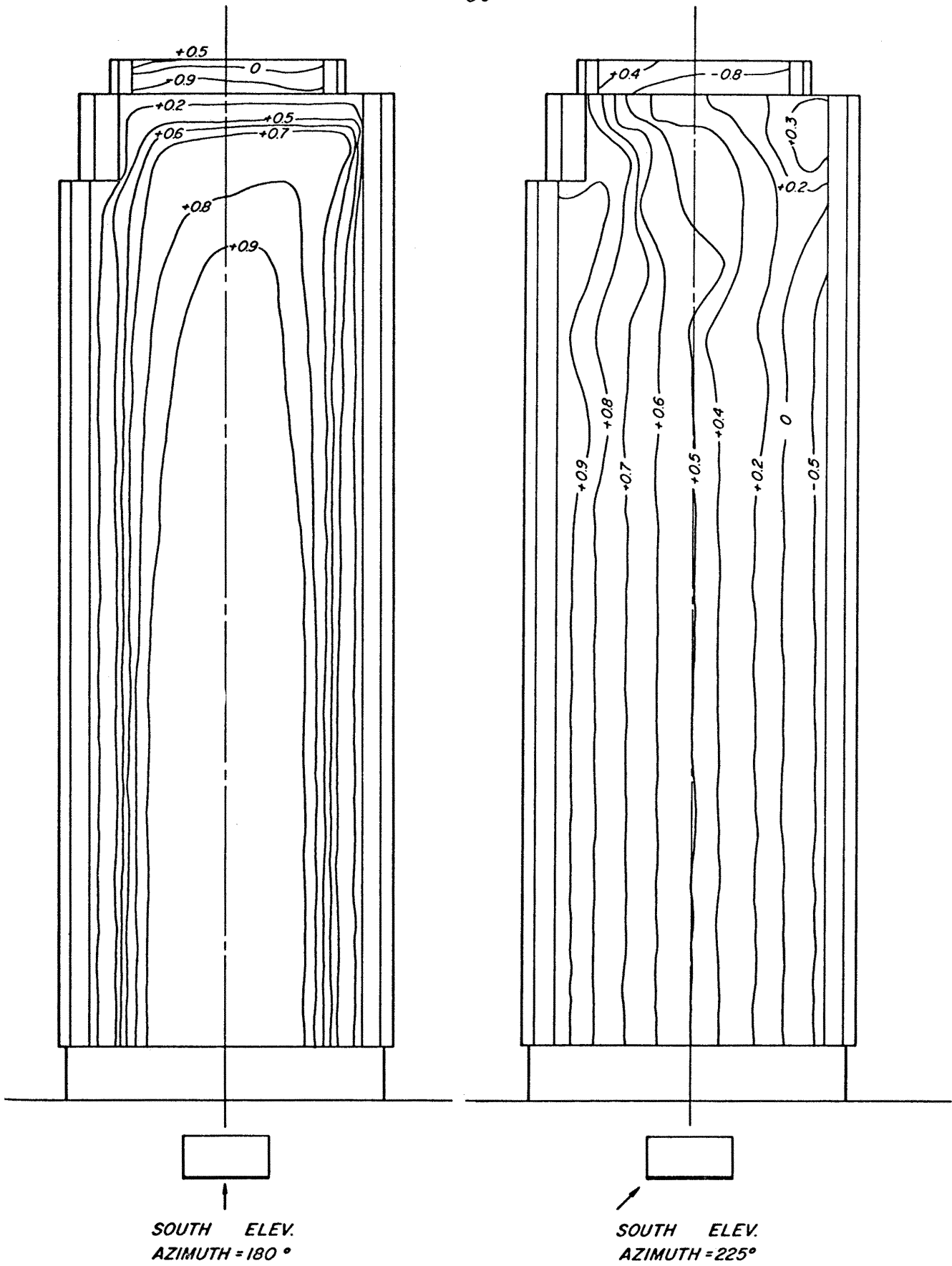


Fig. 15 Pressure Coefficient Distribution-South Side

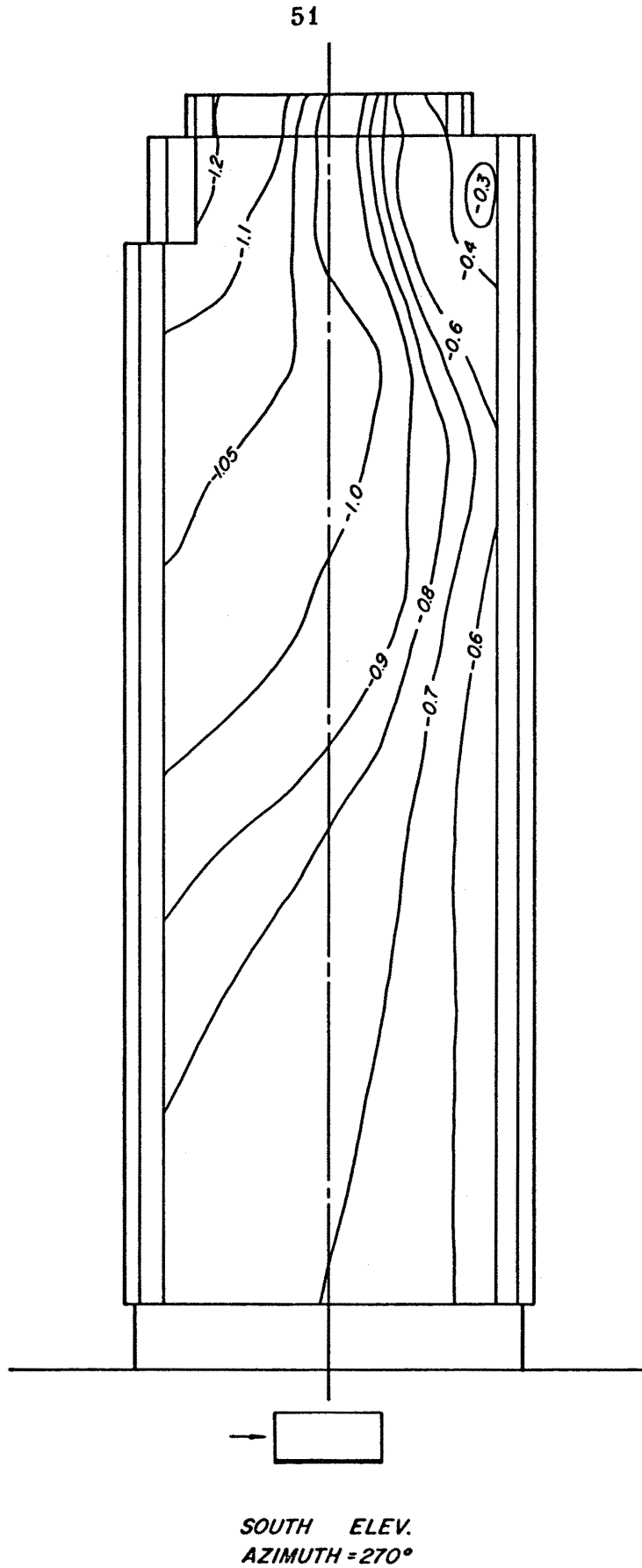


Fig. 16 Pressure Coefficient Distribution-South Side

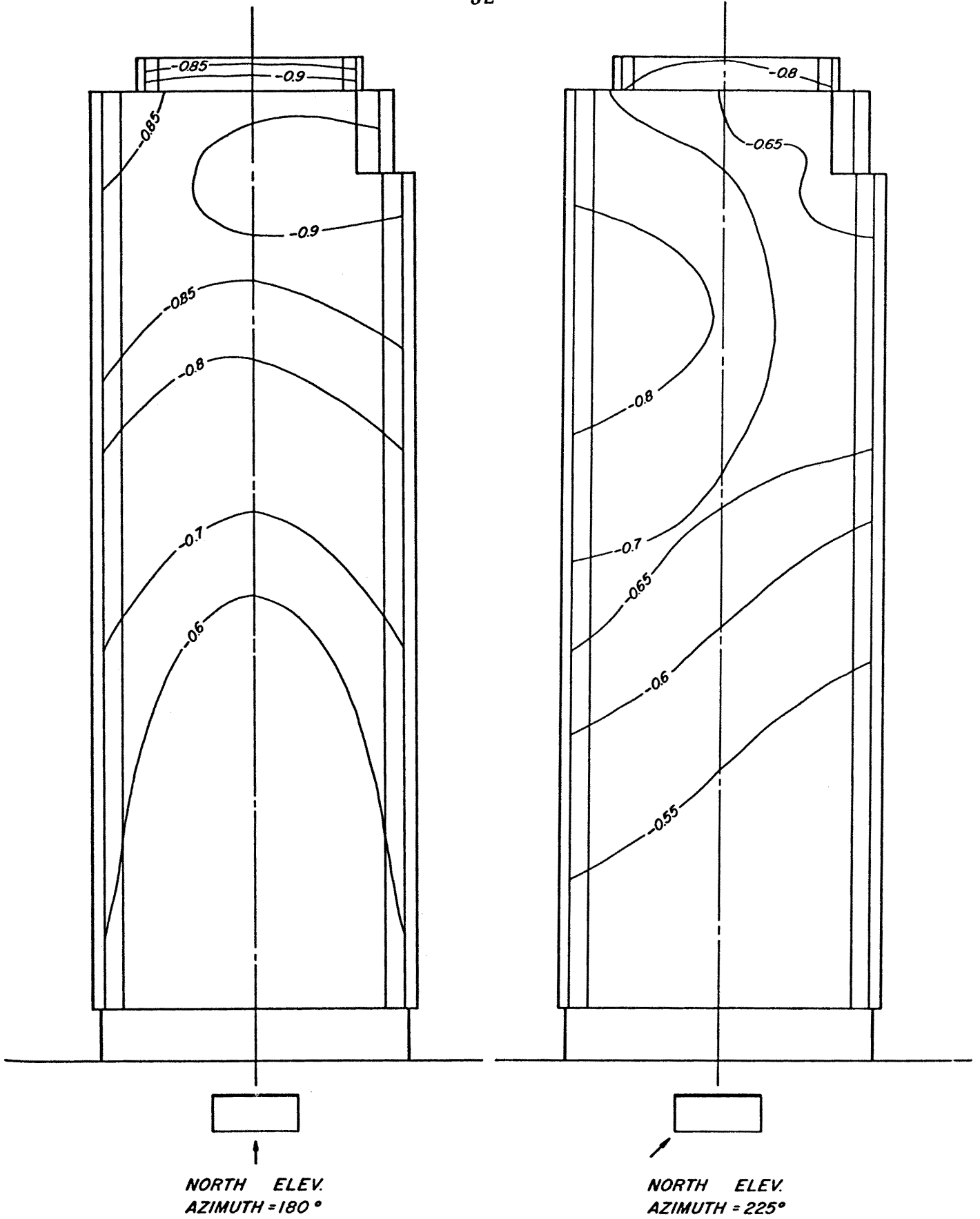


Fig. 17 Pressure Coefficient Distribution-North Side

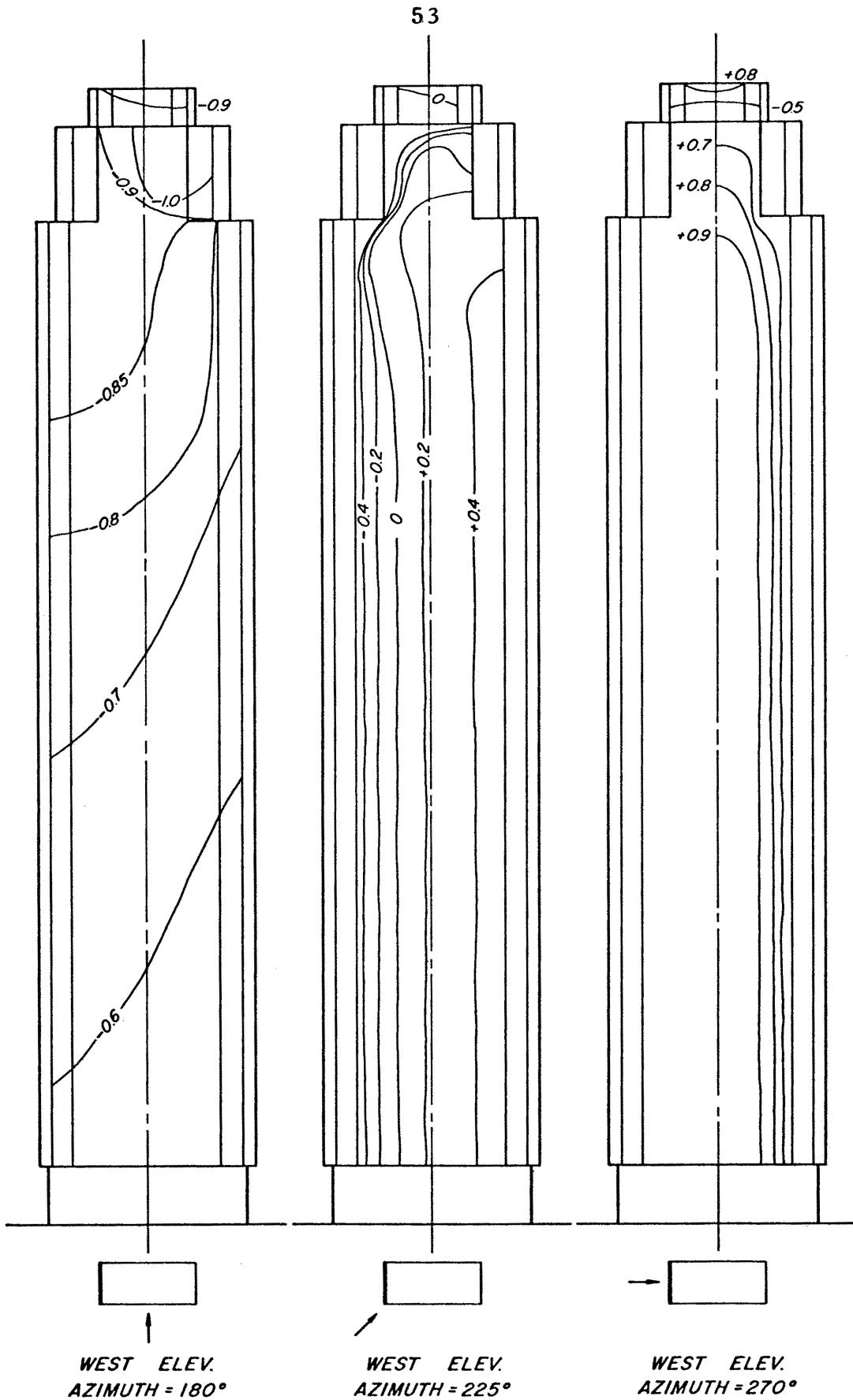


Fig. 18 - Pressure Coefficient Distribution-West Side

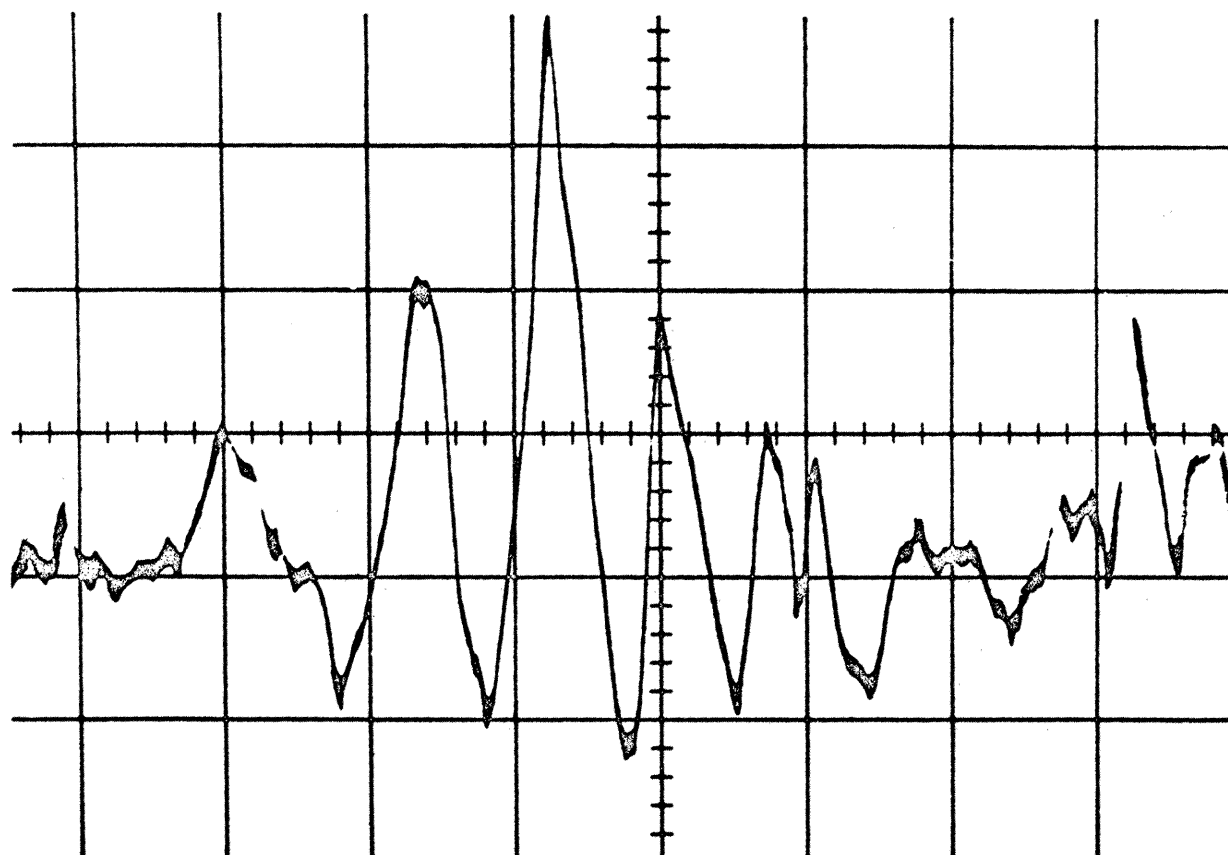


Fig. 20 Oscillogram
Surface Pressure - Difference Fluctuation
Each large horizontal division = 20 milliseconds
Each large vertical division = 0.20 mm Hg.

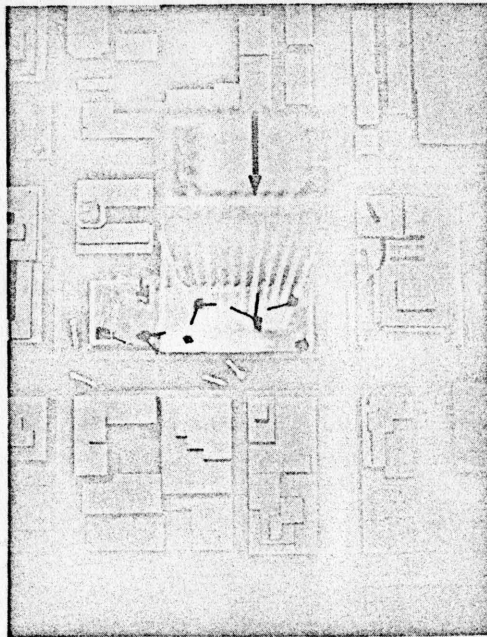
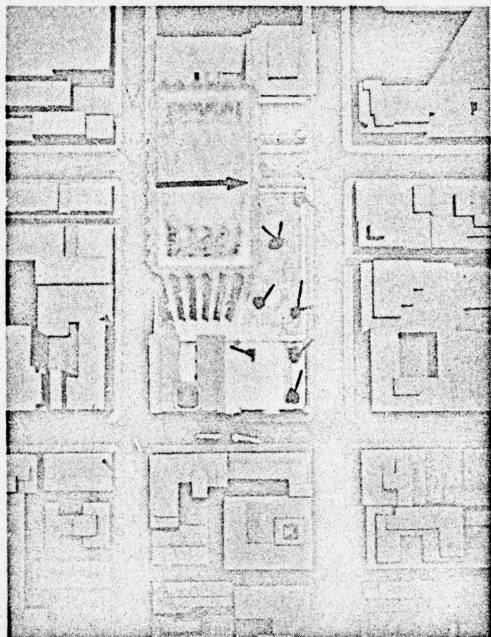


Fig. 21 (a) $U_0 = 30$ ft/sec

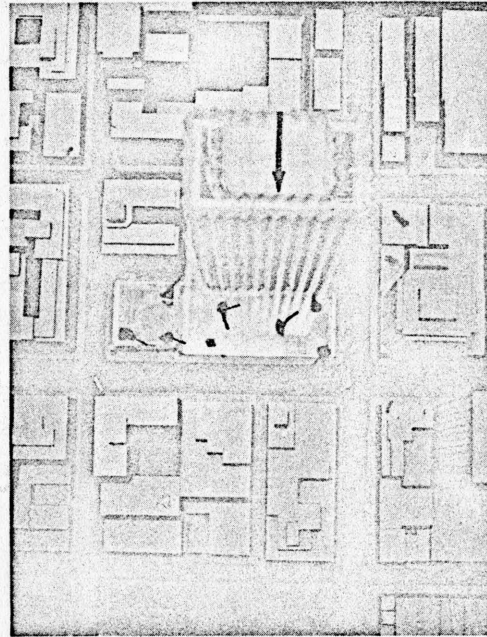
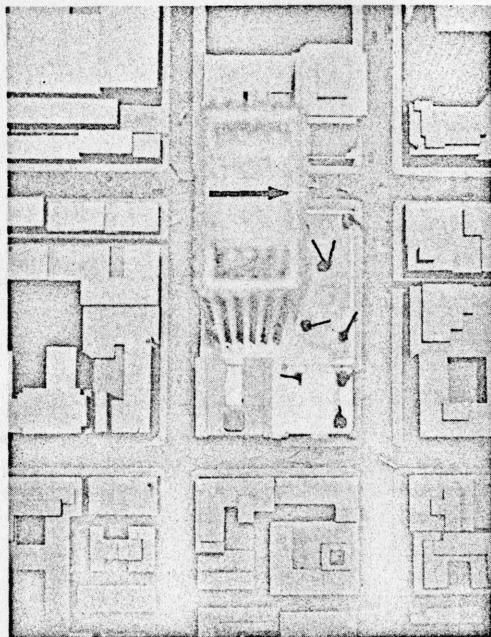


Fig. 21 (b) $U_0 = 60$ ft/sec

Flow Pattern
Azimuth = 180°

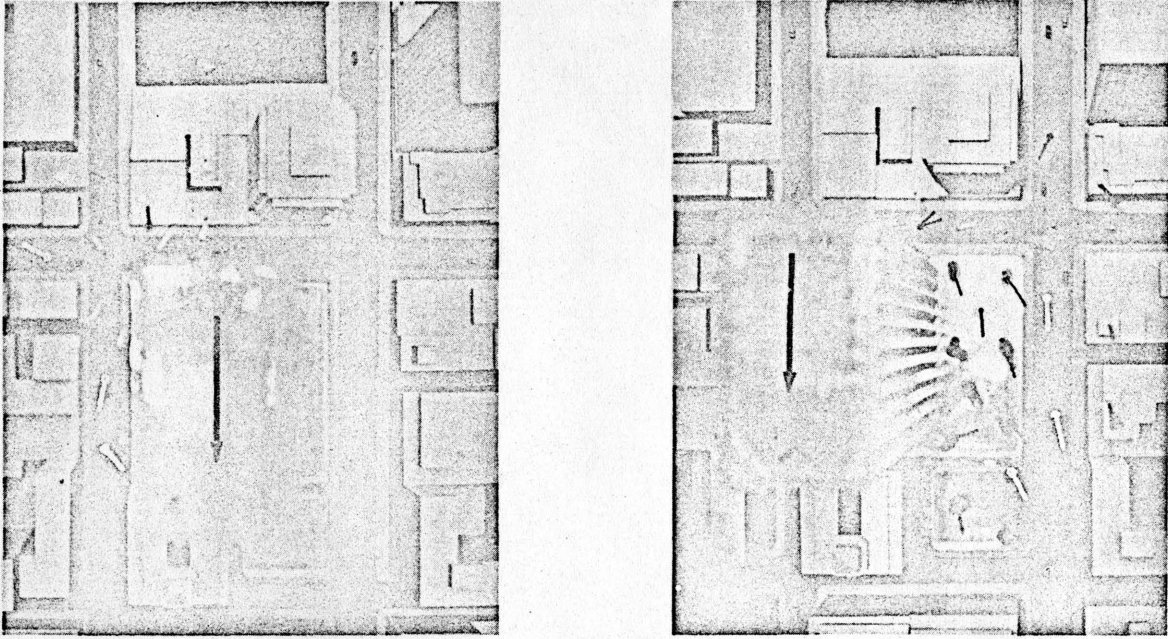


Fig. 22 (a) $U_0 = 30$ ft/sec

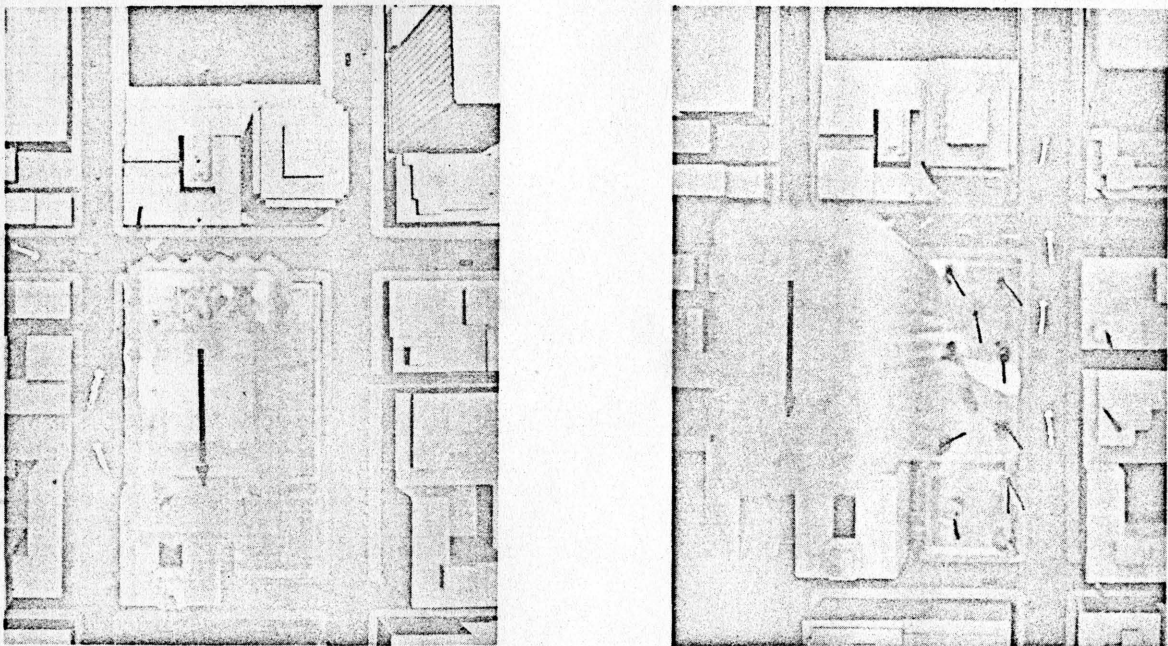


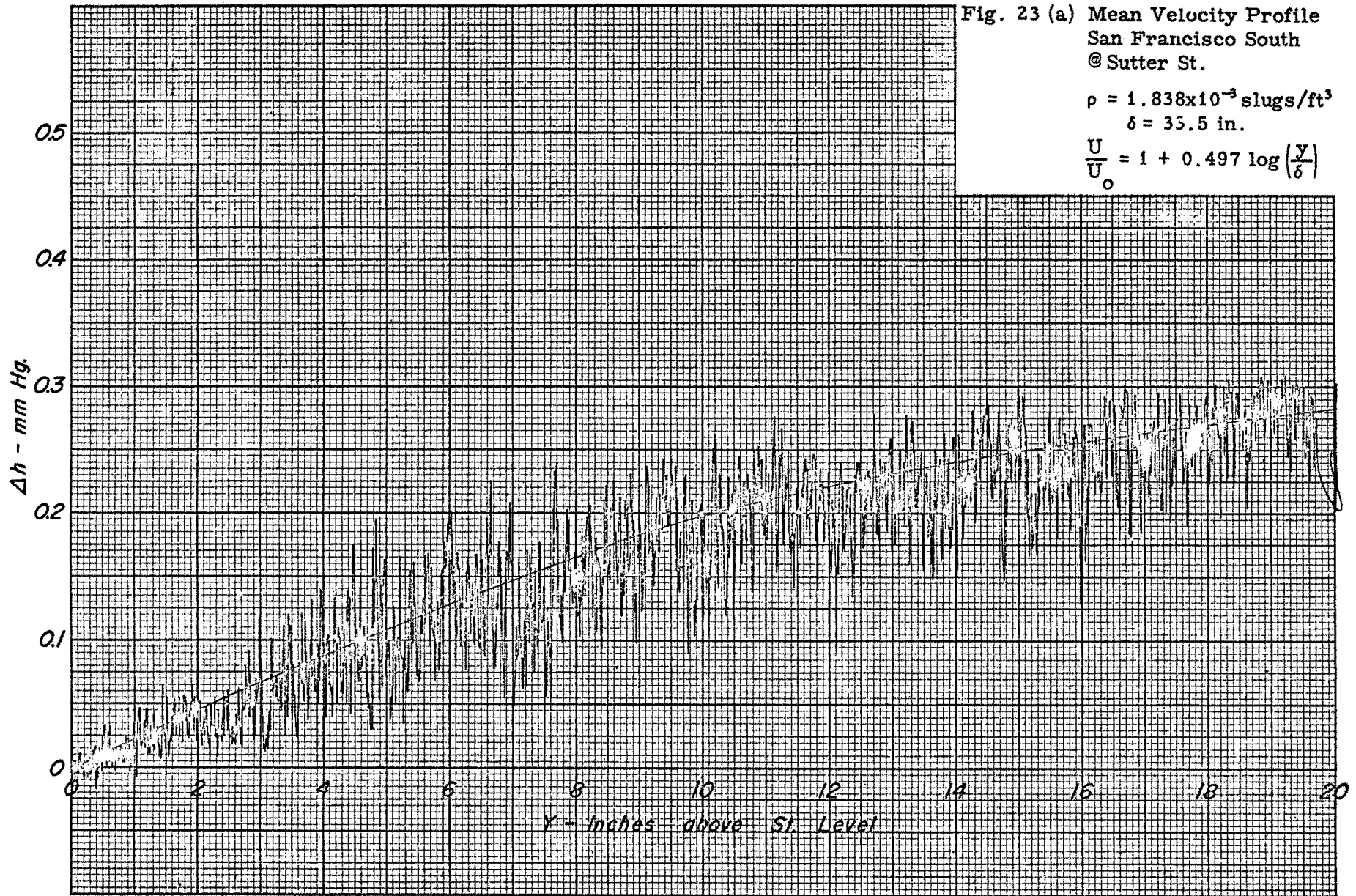
Fig. 22 (b) $U_0 = 60$ ft/sec

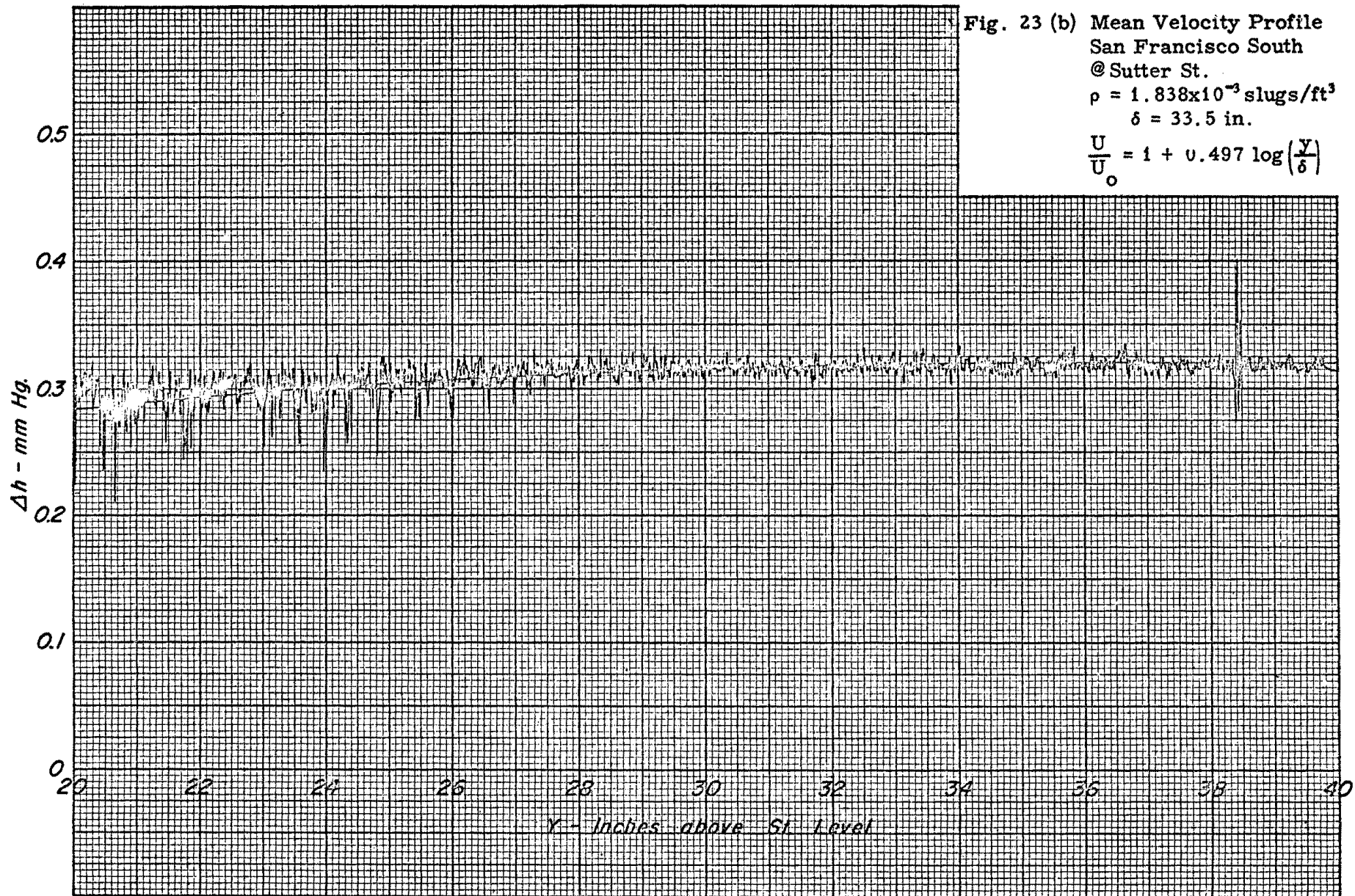
Flow Pattern
Azimuth = 270°

Fig. 23 (a) Mean Velocity Profile
San Francisco South
@ Sutter St.

$$\rho = 1.838 \times 10^{-3} \text{ slugs/ft}^3$$
$$\delta = 35.5 \text{ in.}$$

$$\frac{U}{U_0} = 1 + 0.497 \log \left(\frac{y}{\delta} \right)$$





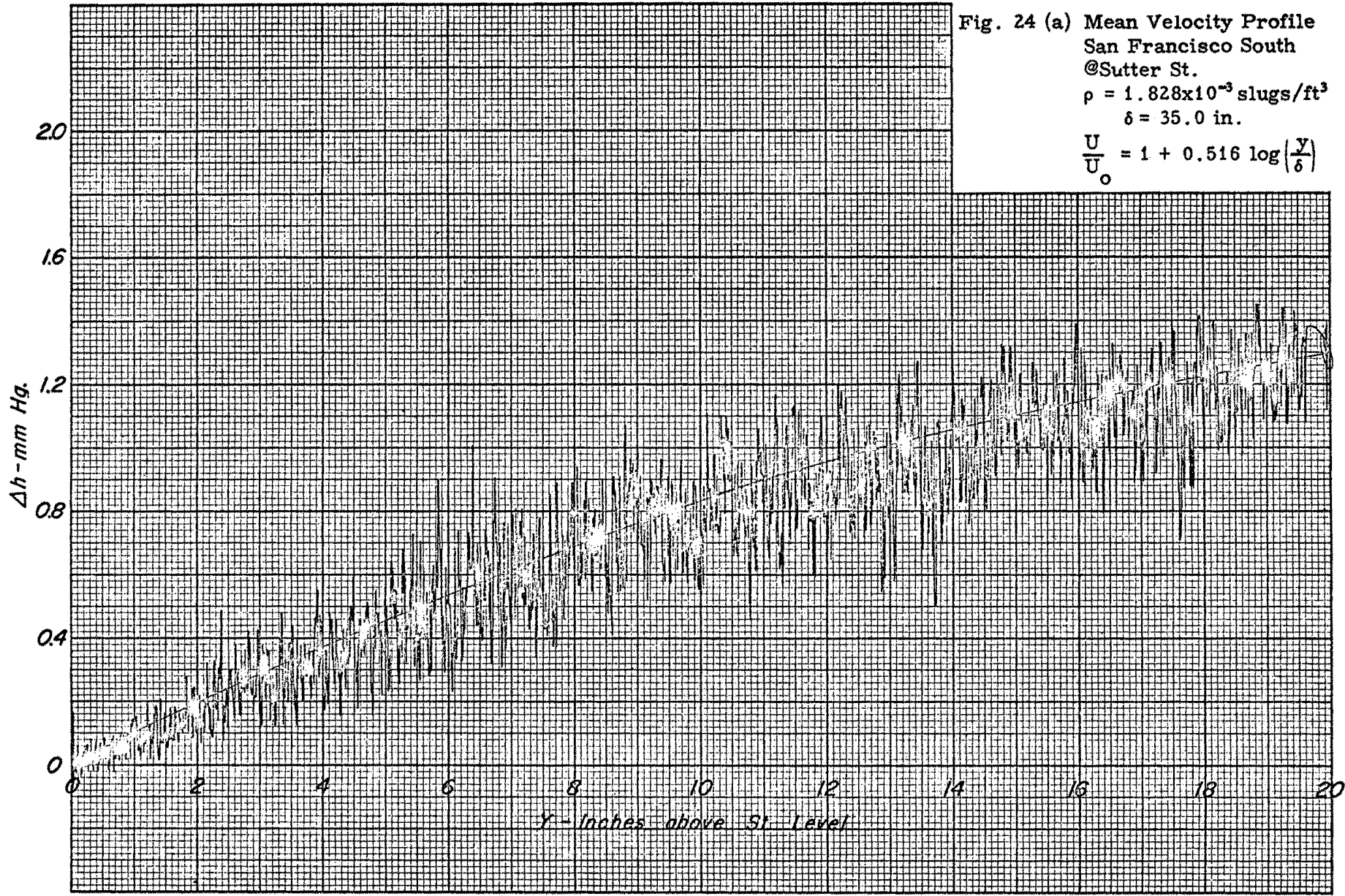
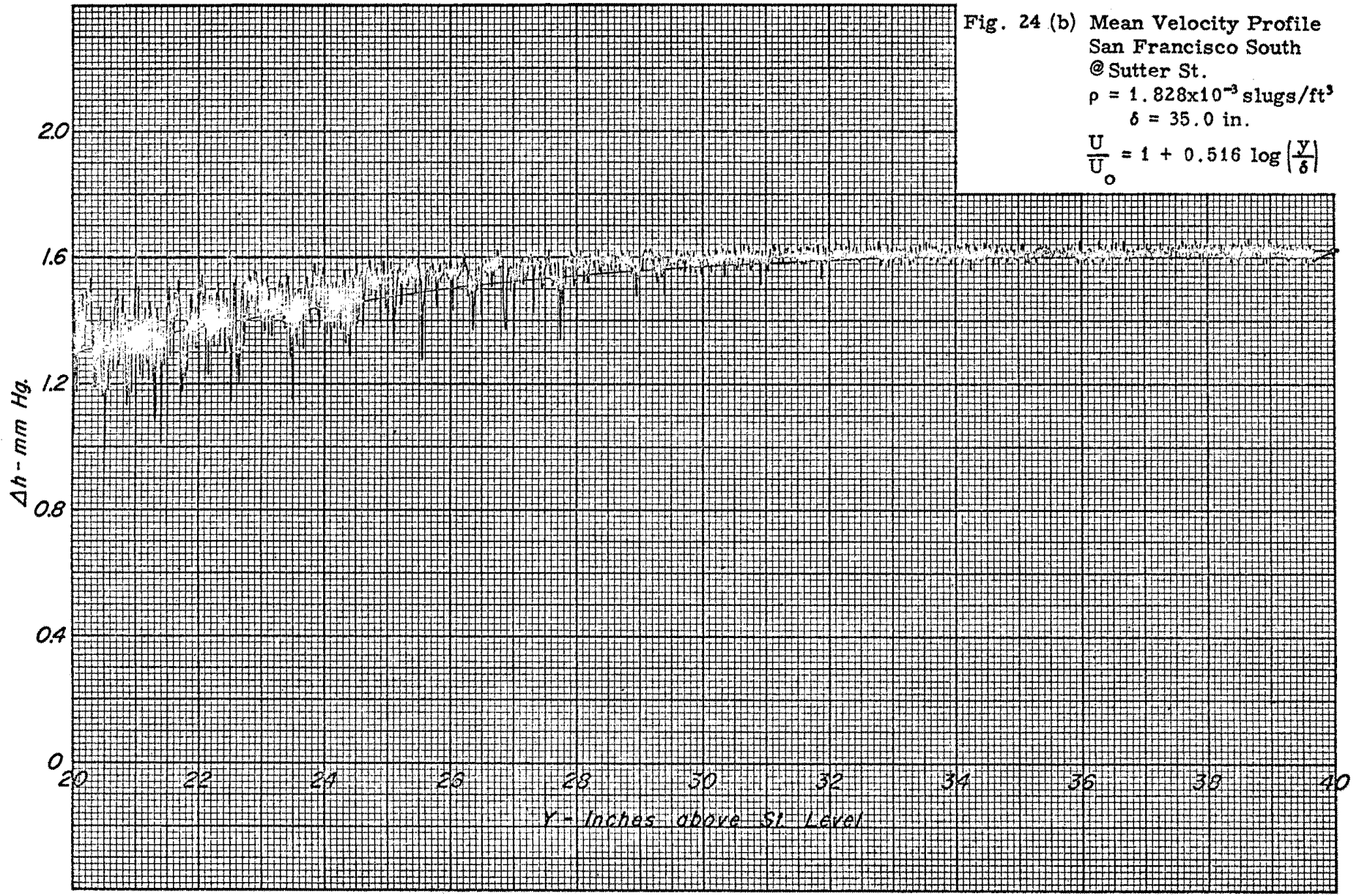


Fig. 24 (a) Mean Velocity Profile
 San Francisco South
 @ Sutter St.
 $\rho = 1.828 \times 10^{-3}$ slugs/ft³
 $\delta = 35.0$ in.
 $\frac{U}{U_0} = 1 + 0.516 \log \left(\frac{y}{\delta} \right)$

Fig. 24 (b) Mean Velocity Profile
 San Francisco South
 @ Sutter St.
 $\rho = 1.828 \times 10^{-3}$ slugs/ft³
 $\delta = 35.0$ in.
 $\frac{U}{U_0} = 1 + 0.516 \log \left(\frac{y}{\delta} \right)$



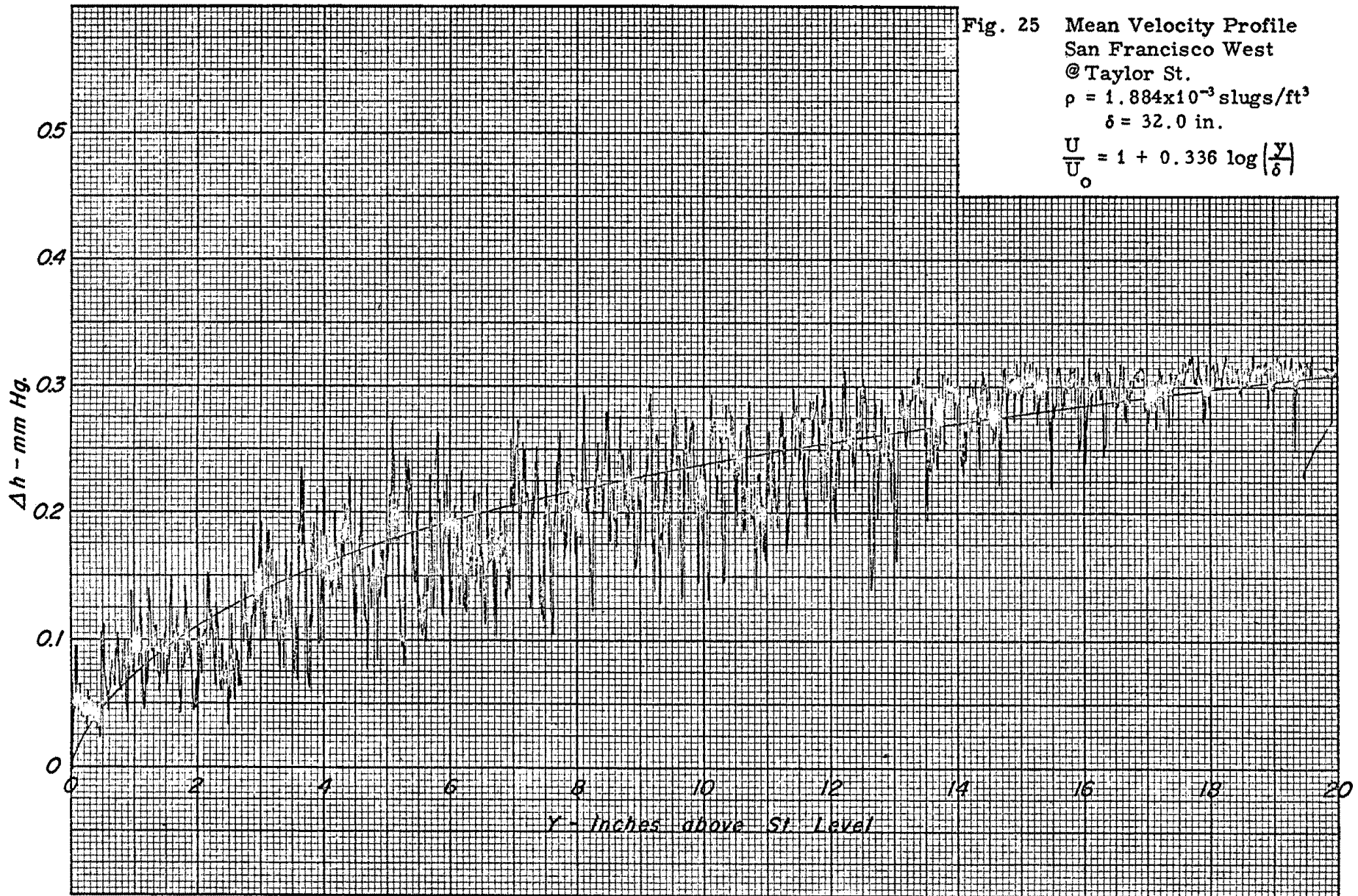


Fig. 26 (a) Mean Velocity Profile
San Francisco West
@ Grant St.

$\rho = 1.884 \times 10^{-3} \text{ slugs/ft}^3$
 $\delta = 30.5 \text{ in.}$

$\frac{U}{U_0} = 1 + 0.378 \log \left(\frac{Y}{\delta} \right)$

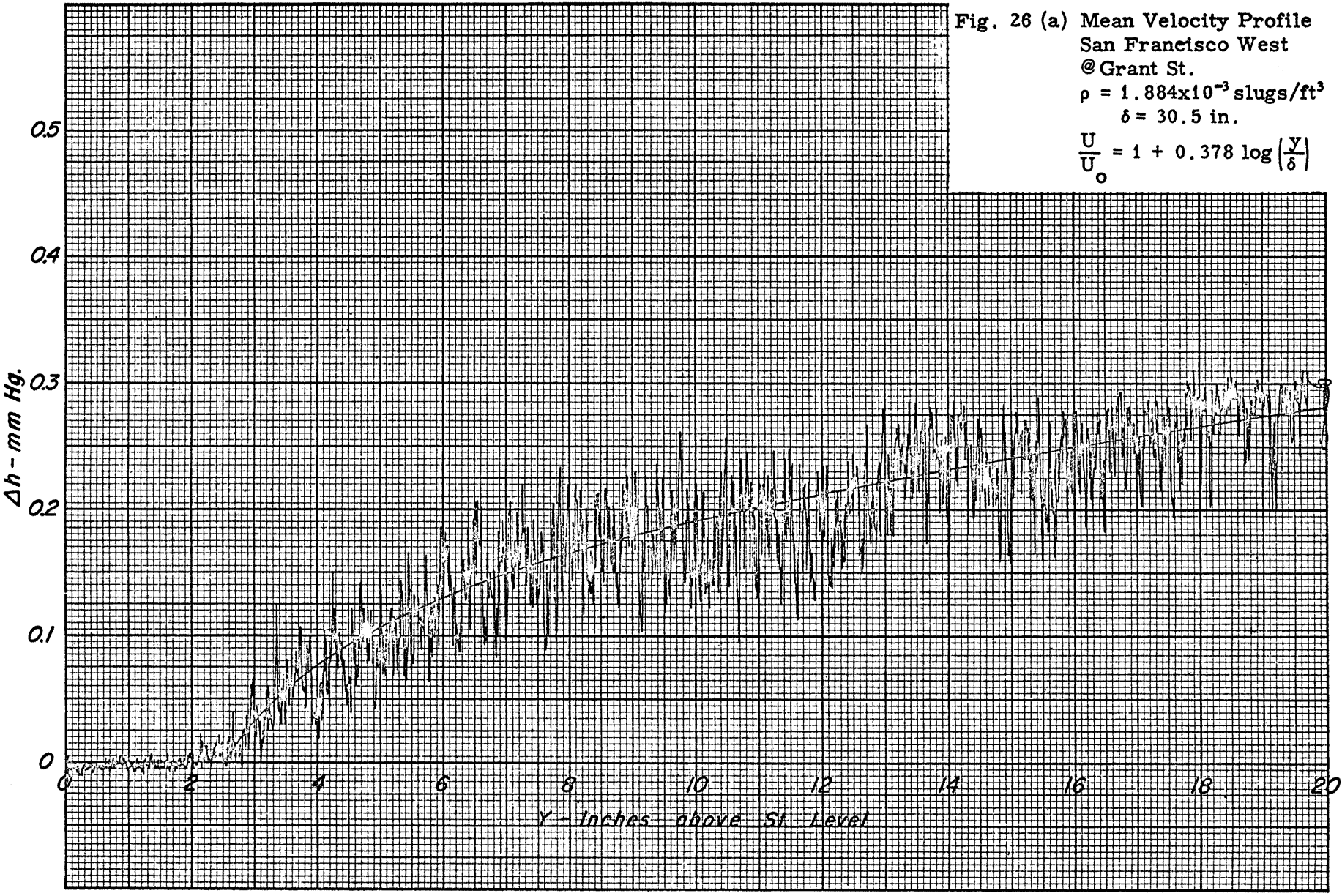
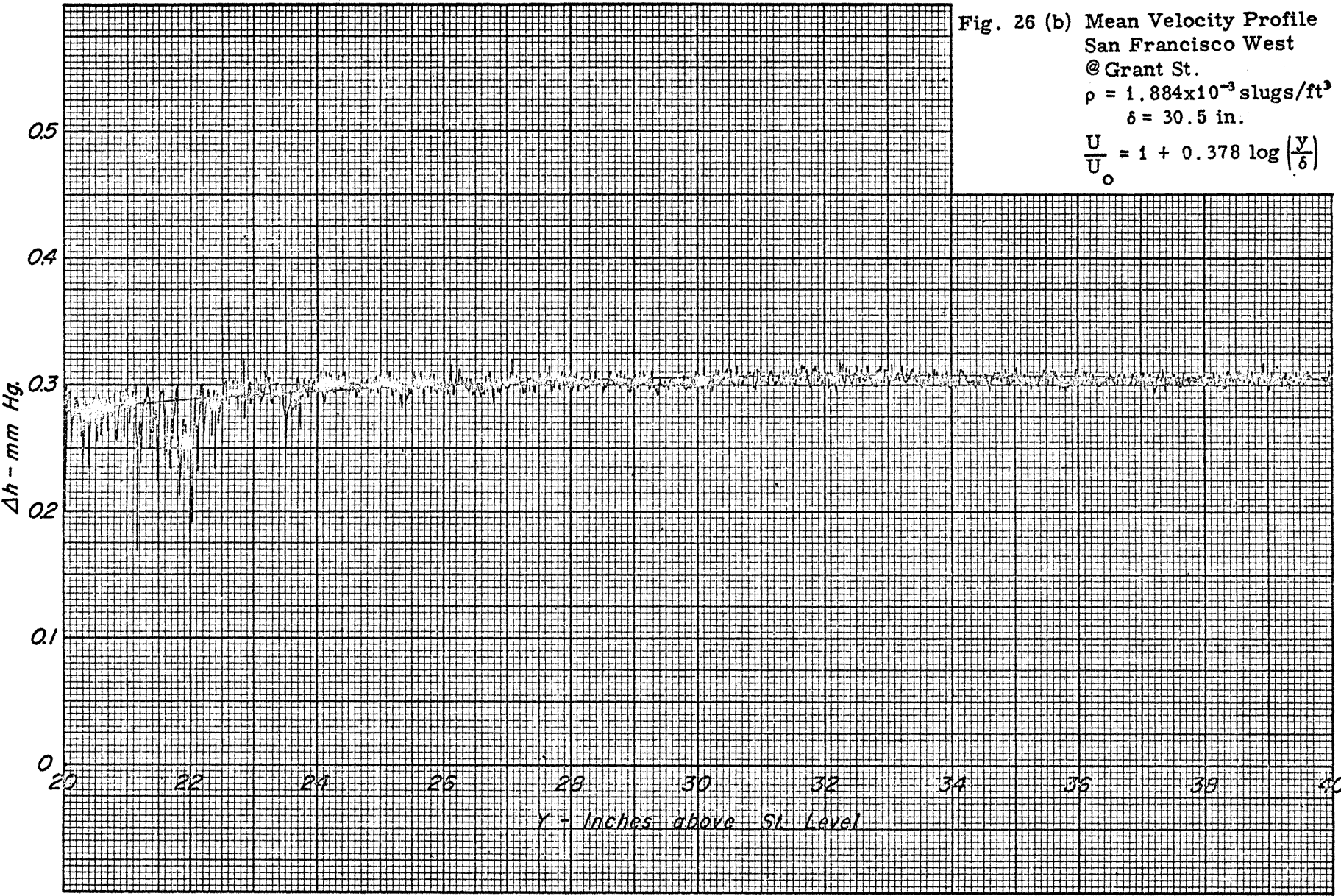


Fig. 26 (b) Mean Velocity Profile
San Francisco West
@ Grant St.

$\rho = 1.884 \times 10^{-3} \text{ slugs/ft}^3$
 $\delta = 30.5 \text{ in.}$

$\frac{U}{U_o} = 1 + 0.378 \log \left(\frac{y}{\delta} \right)$



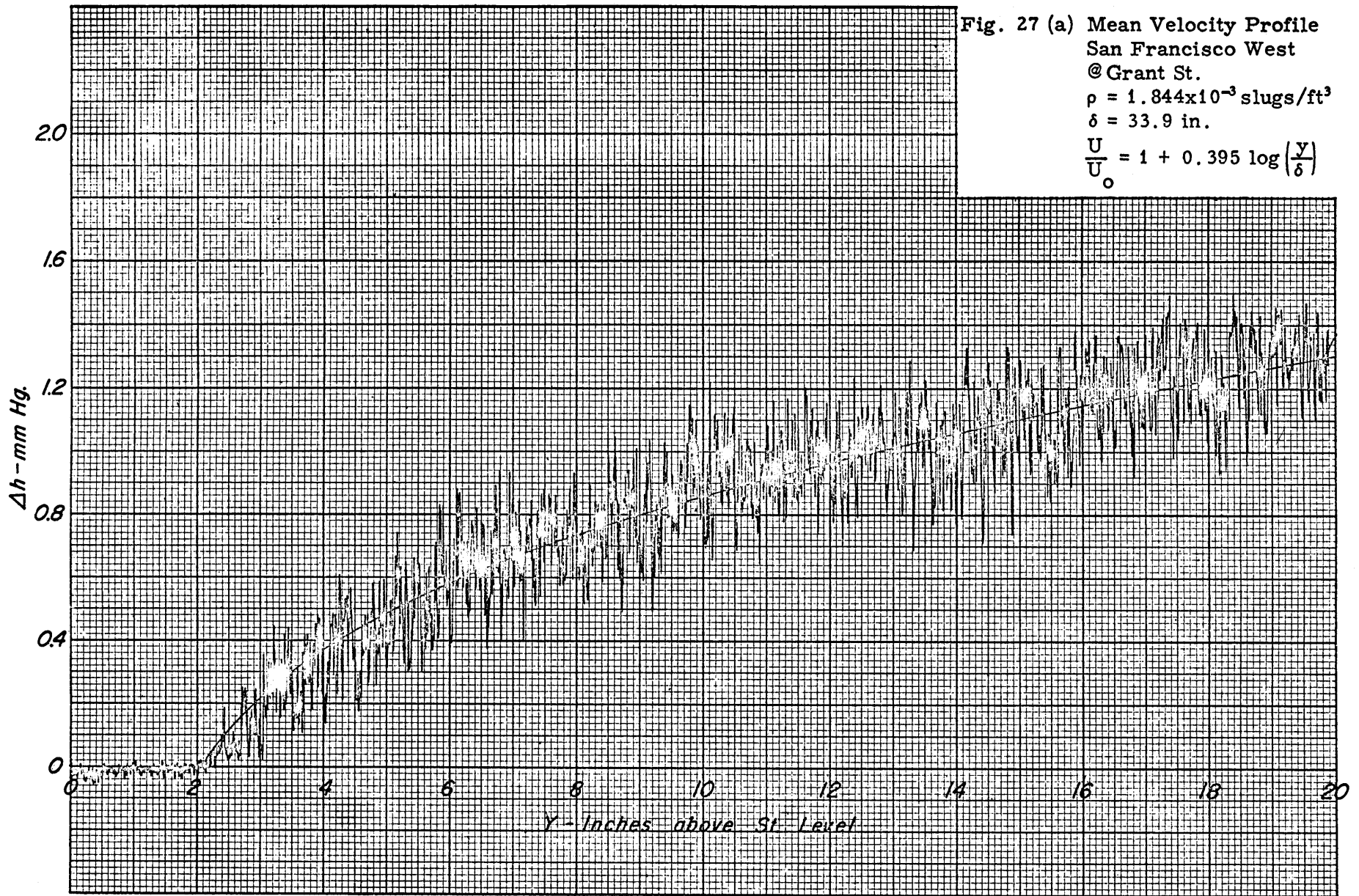


Fig. 27 (b) Mean Velocity Profile
San Francisco West
@ Grant St.
 $\rho = 1.844 \times 10^{-3}$ slugs/ft³
 $\delta = 33.9$ in.
 $\frac{U}{U_0} = 1 + 0.395 \log \left(\frac{y}{\delta} \right)$

